ADVANCED FUNCTIONAL MATERIALS
www.afm-journal.de

Recent Progress in the Synthesis of Spherical Titania Nanostructures and Their Applications

*Dehong Chen and Rachel A. Caruso**

Recent progress in the fabrication and application of diverse spherical titania nanostructures, including mesoporous spheres, spherical flaky assemblies, and dendritic particles of variable diameter and monodispersity in size, is summarized in this article. Utilizing different synthesis strategies, spherical titania nanostructures with tailored polymorphs (including amorphous, anatase, rutile, brookite and TiO_2-B), particle sizes (from tens of nanometers to millimeters), monodispersity, porosity, and variable surface properties have been produced. Such spherical titania nanostructures show realized and potential applications in the areas of chromatographic separation, lithium-ion batteries, dye-sensitized solar cells, photocatalytic oxidation and water splitting, photoluminescence, electrorheological fluids, catalysis, gas sensing, and anticancer intracellular drug delivery. Gaining further understanding of both synthesis design and application of these materials will promote the commercialization of such spherical titania nanostructures in the future.

1. Introduction

Spherical materials are abundant in our daily lives, in confectionary, exquisite opal gems (periodic arrays of spherical silica colloids), and the versatile latex particles and their derivatives (used in numerous rubber products) to name a few.[1–3] Due to their spherical morphology, these particles have the ability to undergo uniform and close packing, it is possible to tune the surface curvature as well as flowability and, if sufficiently small, the particles are dispersible. Hence, spherical materials have shown numerous real and emerging applications. For example, spherical ceria nanoparticles have demonstrated superior abrasive properties for chemical-mechanical planarization of advanced integrated circuits due to the absence of sharp edges, corners, and apexes. These nanoparticles can polish the silicon wafers in a ball bearing-like manner and reduce the concentration of scratch defects, therefore facilitating the precise and reliable mass-manufacture of chips for nanoelectronics.[4] The close-packing and high tap density of various (sub-)micrometer-sized spheres (e.g., $LiCoO_2$, $LiFePO_4$, carbon, V_2O_5) improved the volumetric energy density and gave excellent rate capability when constructed into electrodes for lithium ion batteries.[5–10] Diverse monodisperse microspheres (e.g., silica, ZrO_2) with controllable particle size, porosity and surface properties have been widely used as packing materials for chromatographic separation for many years because they form mechanically stable packing columns with very good packing reproducibility and reduce the pressure drop over the column.[11–13] Spherical pharmaceutical colloidal particles with different sizes have demonstrated controllable drug dissolution rates as a result of the tunable surface curvature, making them superior candidates with enhanced therapeutic effectiveness to the conventional faceted crystallite counterparts.[14,15] Non-agglomerated spherical phosphor nanoparticles with a narrow size distribution and much improved screen packing properties gave superior definition and brighter cathodoluminescent performance in photoluminescent applications compared to irregular morphologies.[16,17]

As an important oxide with numerous practical applications and industrial interest, titania (TiO_2) has attracted significant attention since its commercial production in the early 20th century as a replacement to the toxic lead oxides as a white pigment for paints. Titania is widely used as an inorganic pigment (annual production of >4 million tons) in paints, plastics, paper, leather, textiles, foods and personal care products (e.g., toothpastes, sunscreen creams, and diverse cosmetic products).[18–20] Continuing titania research is exploring novel and highly promising applications including chromatographic separation, photocatalytic redox reactions and water splitting, dye-sensitized solar cells (DSCs), lithium ion batteries, gas sensors and drug delivery vehicles.[13,19–26] Evidence indicates that the efficacy of titania can be varied by its crystal phase and crystallinity, composition, specific surface area and porosity, and importantly, morphology.[27–37] Spherical titania nanostructures with controllable physical and surface properties (including crystal phase, particle size, monodispersity, specific surface area, porosity and surface features) have demonstrated high performance and versatility in a series of applications. For example, spherical anatase beads featuring high specific surface areas and variable

Dr. D. H. Chen, Prof. R. A. Caruso
Particulate Fluids Processing Centre
School of Chemistry
The University of Melbourne
Melbourne, Victoria, 3010 Australia
E-mail: rcaruso@unimelb.edu.au
Prof. R. A. Caruso
CSIRO Materials Science and Engineering
Private Bag 33, Clayton South, Victoria, 3169 Australia

DOI: 10.1002/adfm.201201880

particle sizes have recently achieved high performance in DSCs with increased dye-loading, enhanced light scattering properties and improved electron diffusion due to the well interconnected nanoparticulate networks within the beads.[38–47] Micrometer-sized anatase or rutile spheres with variable pore sizes have shown excellent performance as the packing materials for chromatographic separation and selective phosphopeptide enrichment.[11–13,48–53] The high packing density of the spherical titania polymorphs (anatase and TiO_2-B) resulted in enhanced volumetric energy density and rate capability when applied as anodes in lithium ion batteries.[54–57]

The last decade has seen many advances in the fabrication and exploration of emerging applications of diverse spherical titania nanostructures. Hence a comprehensive review of this important functional material would highlight the research in this field and promote commercial utilization of such titania nanostructures in the future. In this feature article, recent advances in the fabrication of spherical titania nanostructures, including mesoporous spheres, spherical flaky assemblies or dendritic particles of diverse diameter and monodispersity in size, are reviewed. The realized and potential applications of these spherical nanostructures are then summarized. Spherical titania hollow structures were not included in this article as there are recent review articles detailing these specific structures.[58–61] The titania polymorphs described here include amorphous, anatase, rutile, brookite and TiO_2-B (bronze) phases. This article brings together the various preparation techniques along with a range of applications of diverse spherical titania nanostructures with tailored properties to give an overview of this very topical and exciting research.

Dr. Dehong Chen received his Ph.D. in chemistry (2006) from Fudan University (China) under the supervision of Prof. Dongyuan Zhao. He is currently a research fellow in the School of Chemistry, The University of Melbourne. He has interests in design and synthesis of porous inorganic materials for energy conversion and storage, environmental pollution control and photocatalysis applications.

Prof. Rachel A. Caruso received her Ph.D. from The University of Melbourne, Australia before working at the Hahn Meitner Institute and the Max Planck Institute for Colloids and Interfaces. She is an Australian Research Council Future Fellow with research groups in the School of Chemistry, The University of Melbourne and in the Materials Science and Engineering division of CSIRO working on advanced porous materials.

2. Synthesis Techniques

A range of synthesis routes have been applied to obtain porous titania spheres. Here the examples have been brought together under general headings according to the method used: preformed templates, emulsions, aerosols or electrospray that guide the spherical morphology, sol-gel reactions, hydrothermal and solvothermal techniques and finally methods that do not fit these specific categories.

2.1. Templating Method Using Preformed Hard Templates

Porous spherical titania structures have been fabricated using templating methods. This technique makes use of a structured, generally organic material, which holds the required morphology. Chemistry is conducted within the template resulting in a template/titania hybrid, where the titania is commonly amorphous. During a heating step in which the titania is crystallized, the organic material is removed through pyrolysis, thus leaving a titania network with a structure reminiscent of the initial template. Spherical templates that have been applied to the synthesis of titania spheres include porous beads of polystyrene crosslinked with divinyl benzene,[62–64] mesoporous carbon spheres formed themselves through a templating process involving mesoporous silica spheres,[65] and spherical macroporous biopolymer gels (e.g., agarose and alginate).[66–68] In most cases the porous organic spheres were infiltrated with a titania precursor that undergoes hydrolysis within the template structure. The samples were heated between 500 and 600 °C to obtain porous spheres in the anatase phase (higher temperatures, 950 °C, could be used to obtain the rutile phase). Alternatively, preformed titania nanoparticles could be infiltrated within the porous organic sphere and similarly after heating the hybrid sample, produce porous anatase spheres.[63]

The titania beads prepared using sol-gel chemistry within the polystyrene crosslinked with divinyl benzene spheres were monodisperse with a diameter about half that of the original organic sphere, ≈7 or 12 μm. As the sphere is composed of a network of nanoparticles (20–70 nm in diameter), the surface of the sphere and its core are porous (pore size of 50 nm). The specific surface area of these titania spheres was 30–35 $m^2\ g^{-1}$. If hydroxyl or amine-functionalized beads were used, the synthesis of monodisperse titania beads was not successful, as complete precursor infiltration did not occur and excess titania particles (non-templated) formed. Using similar template beads, porous titania spheres with a diameter of 7 μm and surface area of 61 $m^2\ g^{-1}$ were prepared and applied in photocatalytic studies. The degradation of 2-chlorophenol was monitored with time, and although the porous beads were not as active as a commercial titania material, Degussa P25 powder, the ease of

removing micrometer diameter beads over nanoparticles has to be considered.[64]

Hydroxyl functionalized polystyrene crosslinked with divinyl benzene beads having a diameter of 11.5 μm were used for infiltration with preformed titania nanoparticles (4 nm in diameter).[63] The final diameter of the titania beads produced was 5 μm, and the beads were composed of both the anatase and rutile phase with a surface area of 81 m^2 g^{-1}. The photodegradation of 2-chlorophenol at pH 6 was monitored for the beads and compared to Degussa P25 samples. The higher surface area of the beads compared to the Degussa P25 (≈50 m^2 g^{-1}) and the high photoefficiency of the titania sol used to produce the beads were factors attributed to the enhancement in degradation observed with the bead structures.

The thermal and chemical stability, as well as rigidity of carbon made it an attractive template for a range of inorganic beads.[65] Mesoporous silica beads were first produced following Unger's method,[69] within which carbon was synthesized then the silica was removed leaving mesoporous carbon beads. Titanium (IV) isopropoxide was infiltrated within the carbon beads and they were exposed to atmospheric moisture to undergo hydrolysis. The carbon was removed during the calcination step (after the inorganic species had undergone crystallization) by changing the gas atmosphere from nitrogen to air. The beads were 500–600 nm in diameter, were composed of 10 nm nanocrystals, and contained pores of 6 nm. Increasing the temperature of calcination resulted in the rutile phase being present in the final beads.

Beside the individual spherical entities, ordered arrays of mesoporous titania microspheres were also successfully fabricated through a sol-gel self-assembly process confined within a reverse opal template.[70] To prepare such microsphere arrays, templates with ordered void spaces were fabricated by polymerizing methyl methacrylate (PMMA) in an opal structure made of sub-micrometer sized monodisperse silica spheres (**Figure 1**). The silica was removed using 10 wt% HF solution (24 h) to obtain a freestanding PMMA reverse opal mesh that was used as a template in which the sol-gel chemistry was conducted in the presence of the Pluronic P123 triblock copolymer. Calcination at 400 °C in air removed the PMMA template and the triblock copolymer surfactant giving ordered arrays of mesoporous titania microspheres. The spheres were composed of anatase nanocrystals and possessed a high specific surface area of 145 m^2 g^{-1} and a narrow mesopore centered at 3.6 nm.

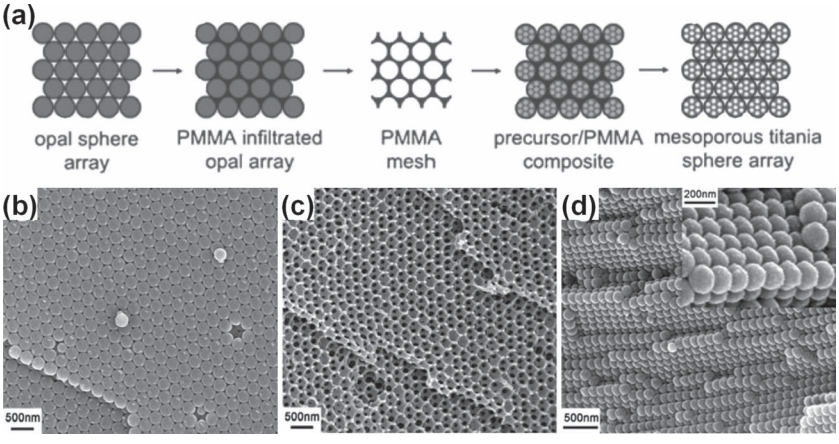

Figure 1. a) Schematic of the fabrication process for titania microsphere arrays templated using PMMA reverse opal mesh. b) SEM image of the opal structure made of 290 nm silica spheres. c) SEM image of the PMMA mesh derived from the silica opal structure. d) SEM image of the replicated mesoporous titania microsphere array. Inset in (d) shows a higher magnification image of the titania microsphere array. Adapted with permission.[70] Copyright 2010, Royal Society of Chemistry.

2.2. Emulsion-Mediated Synthesis

Spherical sub-micrometer-sized titania clusters consisting of ultrafine anatase nanodots or nanorods can be fabricated via an emulsion (oil-in-water) assisted self-assembly process.[52,53,71–73] To prepare such spherical titania clusters, ligand-capped hydrophobic anatase nanocrystals in a low-boiling-point organic solvent (e.g., cyclohexane) were dispersed in water to form an oil-in-water emulsion with the aid of a surfactant (e.g., sodium dodecyl sulphate) and ultrasonic dispersion. The organic solvent, cyclohexane, in the oil droplets was evaporated by heating the solution at 70 °C for a period of time (usually several hours), causing the nanocrystals confined in the oil droplets to self-assemble into spherical clusters. Calcination in air (usually at 400 or 500 °C) was conducted to remove the organic ligand and enhance mechanical stability of the resulting titania clusters. Yin and co-workers recently found that a silica coating on the resulting titania clusters prior to calcination can prevent aggregation during the thermal treatment and retains the spherical morphology of the products; the pre-coated silica layer can be readily etched away using a dilute NaOH solution after calcination.[52,53,73] The diameters of these clusters can be controlled by adjusting the titania nanocrystal concentration in the organic solvent, surfactant concentration in the water phase, oil-to-water ratio or the extent of sonication during emulsification. Spherical titania clusters having specific surface areas of up to 441 m^2 g^{-1} and an average pore diameter of 3.5 nm have been prepared using anatase nanorods (3 nm × 28 nm). These properties vary with the crystal size of the anatase building blocks and calcination temperature. Such titania clusters are highly promising for selective enrichment of phosphorylated peptides in phosphoproteome analysis. Hybrid titania clusters containing magnetic iron oxide nanoparticles or quantum dots (e.g., CdSe) can also be fabricated via this facile emulsion assisted self-assembly process.[52,53,72]

Reverse water-in-oil emulsions, formed by dispersing an aqueous suspension of titania nanoparticles into hexadecane (oil phase) using a drop break-off technique in a co-flowing stream, were employed to confine the assembly of the preformed titania nanoparticles within the droplets geometry.[74] Yang and co-workers found that the diameter of the titania microspheres (d_m) can be

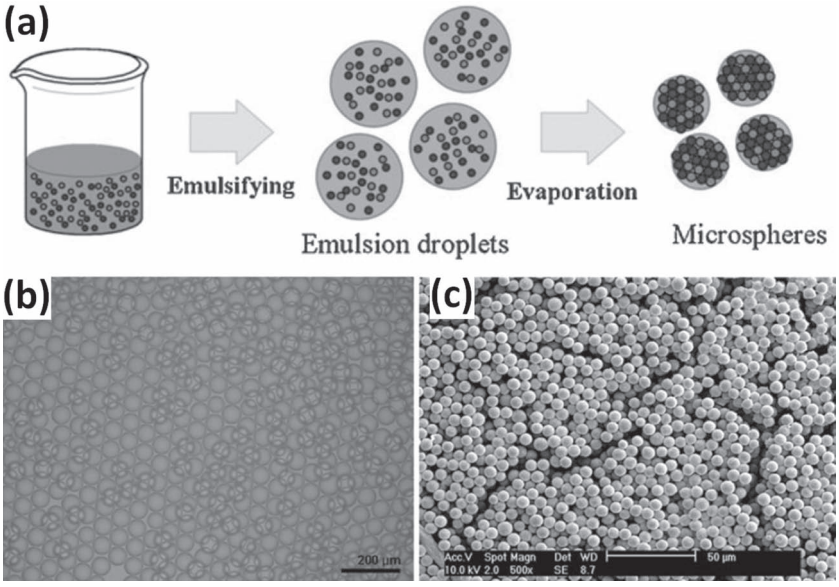

Figure 2. a) Schematic of the microemulsion-assisted self-assembly process for titania microspheres. b) Optical microscopy image of the uniform emulsion droplets with an average diameter of 60 μm that were obtained from micropipettes with an inner diameter of 10 μm. Titania nanoparticle content in the aqueous suspension was 0.2 wt%. c) SEM image of titania microspheres with an average diameter of 7 μm after evaporation induced consolidation. Adapted with permission.[74]

controlled by the inner diameter of the micropipette (d_t) and weight fraction of the titania nanoparticles in suspension (φ_w), as follows,

$$d_m \propto d_t \phi_w^{1/3}$$

Using a colloidal suspension consisting of pre-mixed nanoparticles (e.g., silica and titania) as the precursor (**Figure 2**), fairly monodisperse composite microspheres with different component weight ratios, surface roughness and tunable refractive indexes can be fabricated via this process. Pre-mixing organic dye molecules with the aqueous colloidal suspension gives coloured titania microspheres with a homogeneous dye distribution inside the sphere that may be applied as biological probes. Using a reverse emulsion-mediated synthesis method, Tartaj reported the synthesis of spherical titania mesocrystalline assemblies by mixing aqueous $TiOSO_4$ solution, Igepal CO-520 (surfactant) and cyclohexane (continuous oil phase).[75] The resulting products have a diameter ranging from 50 to 70 nm and variable surface area and pore size. The titania assemblies synthesized at 80 °C have a specific surface area of ≈250 m^2 g^{-1} and a pore size around 2.5 nm, while those prepared at 120 °C possess a specific surface area of ≈200 m^2 g^{-1} and a pore size around 4 nm. Landfester and co-workers prepared porous titania nanospheres (≈200 nm in diameter) via an inverse miniemulsion method using a water-soluble glycol-modified precursor (bis(2-hydroxyethyl)titanate) dispersed in a continuous organic phase containing a home-made block copolymer surfactant and an organic solvent (Isopar M).[76] Porous nanospheres consisting of ≈5 nm titania nanocrystals and having a high surface area of 321 m^2 g^{-1} were fabricated in the presence of 5 wt% block copolymer surfactant.

2.3. Aerosol-Assisted Self-Assembly Method

The aerosol-assisted self-assembly method, an integration of aerosol spray, sol-gel chemistry and evaporation-induced self-assembly processes,[77,78] is a versatile approach for the fabrication of spherical particles with varied size, porosity and composition.[54,79–84] Aerosol (liquid droplets dispersed in a carrier gas) of the precursor solution usually containing titanium species, surfactants and solvents can be generated by a powerful air jet, ultrasonic nebulizer or other means. The resultant aerosol was carried by the carrier gas through a tubular heating chamber to remove solvent and volatile solutes, and initialize the self-assembly between titanium species and surfactant molecules, giving rise to condensed spherical particles with robust frameworks (**Figure 3**a). This is a continuous process and the aerosol remains at high

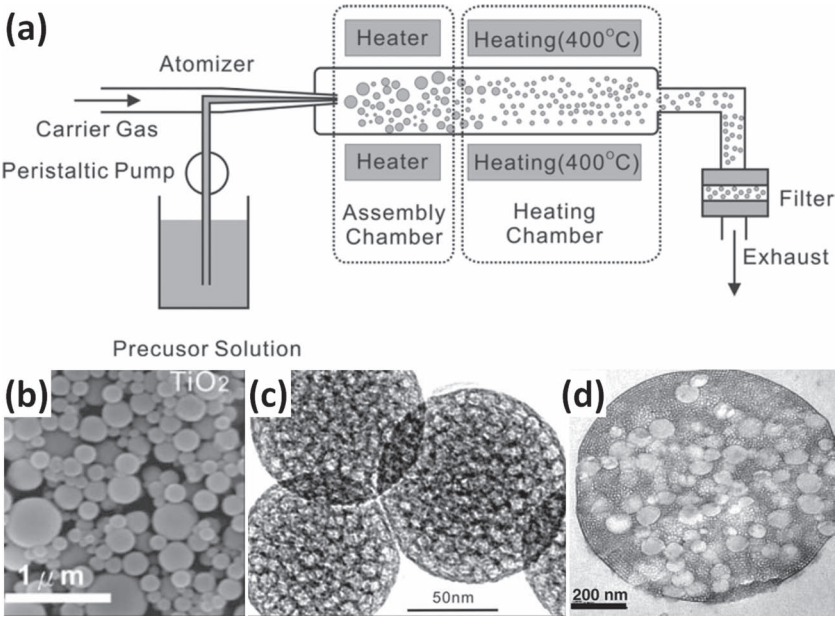

Figure 3. a) Schematic of the aerosol-assisted self-assembly process for spherical titania particles. b) SEM and c) TEM images of the typical mesoporous titania microspheres. d) TEM image of an ultramicrotomed titania microsphere prepared in the presence of latex spheres as porogens for the macropores (the larger white spots). Panel (a) reproduced and panels (b,c) adapted with permission.[81] Panel (d) reproduced with permission.[84]

temperature for a short period (usually several seconds) before being collected. A subsequent thermal treatment is essential to totally remove the organic surfactants and to further condense the inorganic framework. Wang and co-workers fabricated titania sub-micrometer sized spheres composed of anatase nanocrystals less than 10 nm in size using a precursor solution containing hydrolyzed titanium (IV) butoxide, acetic acid, amphiphilic block copolymer (Pluronic F127), HCl, ethanol and water (Figure 3b,c).[81] The titania spheres possess a short-range mesoscopic order, specific surface area of 237 $m^2 g^{-1}$ and pore diameter of 4.8 nm when calcined at 350 °C for 5 h.[81] Increasing the calcination temperature to 400 °C, the specific surface area decreased to 154 $m^2 g^{-1}$ due to coarsening of the titania nanocrystals. The composition of these titania spheres can be readily adjusted by adding other metal species, such as $Cu(NO_3)_2$, $EuCl_3{\cdot}6H_2O$, $SmCl_3{\cdot}6H_2O$, $HAuCl_4$, H_2PdCl_4, and H_2PtCl_6 into the precursor solution.[81–83] Apart from the diverse surfactants employed as the porogens for mesoporosity, other relatively large porogens, such as latex colloids, can be added into the precursor solution to synthesize titania microspheres containing multiscale porosities via this method (Figure 3d).[84] Yamauchi and co-workers found that this aerosol-assisted self-assembly method is more suitable for continuous production of mesoporous titania microspheres on a large scale by using a cyclone separator, rather than a filter, to collect the final products.[85] The titania microspheres fabricated via this aerosol-assisted self-assembly process usually have a broad particle size distribution ranging from tens of nanometers to several micrometers.[54,81–88] In order to obtain relatively monodisperse particles, a size-partitioning process, such as density gradient centrifugation,[88] is generally exploited.

2.4. Electrospray Method

A schematic of the electrostatic spray process and typical morphology of the resultant product are shown in **Figure 4**. For this synthesis, a homogeneous dispersion that usually contains partially hydrolyzed titanium species or colloids, solvent and binders (optional) is required. This dispersion is loaded into a syringe pump and forced through the nozzle under a direct electric field applied between the metal nozzle and the collection substrate. The resulting detached droplets are generally collected on the substrate or in an oil solvent. As water and solvent evaporate, the titania colloid and surfactants (binder) can directly self-assemble into robust microspheres. For example, using commercial titania nanocrystals (e.g., Degussa P25) well dispersed in a mixed ethanol-H_2O solvent in the absence of any surfactants and additives, Kim and co-workers prepared mesoporous titania microspheres using this technique.[89,90] These microspheres have diameters ranging from 200 nm to micrometers and can be controlled by tuning the size of the droplets, which is adjusted by diverse process parameters, such as concentration of the suspended nanocrystals, flow rate and voltage applied. Crack-free and uniform titania microsphere films showing enhanced adhesion to the substrates can be directly electrosprayed onto conducting fluorine-doped tin oxide (FTO) glass or flexible substrates via this facile process. Using a similar method, Cao et al. also fabricated polydisperse titania aggregates (0.3–2.5 μm in diameter) using a mixture of Degussa P25 nanocrystals, poly(vinyl pyrrolidone) (PVP, MW ≈ 1.3×10^6 g/mol) in a water–ethanol solution at a flow rate of 0.3 mL h^{-1} and an applied voltage of 12 kV.[91,92] This electrostatic spray process can also be combined with the sol-gel synthesis and solvothermal process to prepare mesoporous titania microspheres with relatively high surface areas (from 108 to 198 $m^2 g^{-1}$) and large pore volume (from 0.31 to 0.67 $cm^3 g^{-1}$).[93] In this case, a mixture of partially hydrolyzed titanium (IV) butoxide, acetic acid, PVP (MW = 25 000 g/mol) and ethanol was loaded into a syringe pump to fabricate the precursor microspheres. The precursor microspheres underwent a solvothermal crystallization in the presence of acetic acid of diverse concentrations. The titania microspheres were composed of anatase nanocrystals with exposed high-energy facets, including step-like {001} and smooth {010} facets. The percentage of exposed {001} facets was adjusted by changing the amount of PVP used in the electrospray process and the concentration of acetic acid added during the solvothermal treatment.

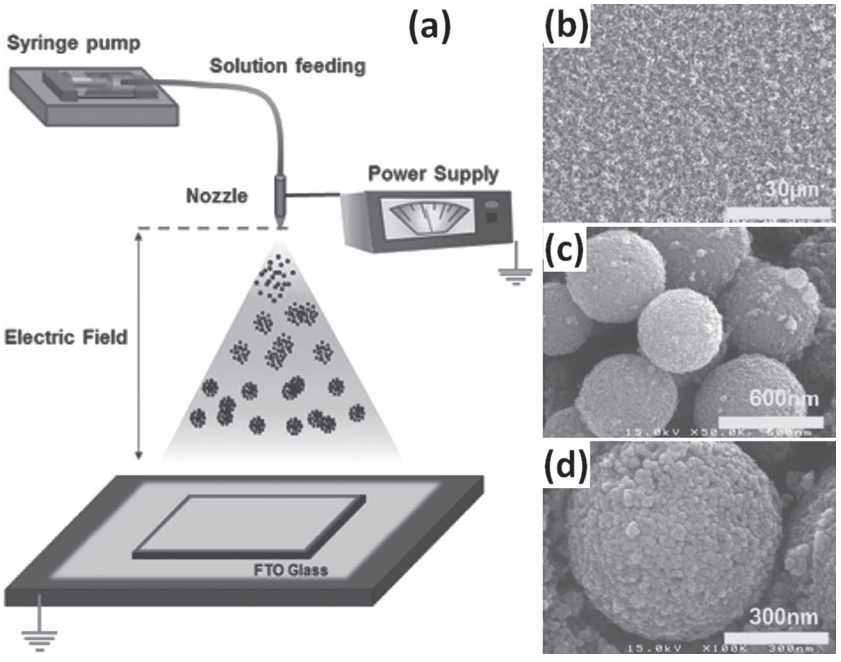

Figure 4. a) Schematic of the electrostatic spray process for titania microspheres. b–d) SEM images of the resultant mesoporous titania microspheres consisting of Degussa P25 nanoparticles. Adapted with permission.[89] Copyright 2011, American Chemical Society.

2.5. Sol-Gel Synthesis

Due to the high reactivity of the titanium alkoxides, sol-gel syntheses of spherical titania colloids were usually conducted in a non-aqueous solvent containing small

amounts of water or in the presence of diverse chelating agents (e.g., acetylacetone or ethylene glycol) to slow down the hydrolysis of alkoxides and allowing more control of the material properties.[94–105] For example, Xia and co-workers developed an ethylene glycol modified sol-gel process to reduce the hydrolysis rate of the titanium alkoxides and thus fabricate monodisperse spherical titanium glycolate colloids with tunable diameters ranging from 200 to 500 nm using acetone containing ≈0.3% water as the solvent.[102] After annealing at 500 or 950 °C for 2 h, the spherical titanium glycolate colloids were readily converted into anatase or rutile sub-micrometer-sized spheres with ≈14% or ≈17% shrinkage in diameter, respectively. The titanium glycolate colloids could also be employed as the building blocks to form 3D opaline lattices through self-assembly in a home-made microfluidic cell. The resulting face-centered cubic opaline lattices were crystallized into an anatase counterpart after annealing at 500 °C for 2 h, with ≈16% volume shrinkage and some cracking in the opaline structure. The authors found that high purity acetone (HPLC grade) played a key role in the formation of monodisperse colloids, as spherical colloids with an inferior monodispersity in size were obtained when replacing acetone with other organic solvents, such as methanol, 1-propanol, 1-butanol, acetonitrile, ethyl acetate, dimethyl sulfoxide and *N*,*N*-dimethyl formamide. Sugimoto and Kojima investigated the formation of monodisperse ≈450 nm amorphous titania spheres by hydrolyzing titanium (IV) butoxide and condensation of the resulting hydroxide monomer in the presence of 0.1 M ammonia aqueous solution using a mixed solvent of butanol and acetonitrile.[95–97] The ammonia can simultaneously accelerate the precipitation of the hydrolyzed hydroxide species, retard the coagulation of the growing hydroxide particles, regulate surface energy of the particles and promote the production of highly spherical particles, clearly demonstrating its versatile multiple roles in controlling the formation of the spherical titania colloids. Beside the ammonia, the water content, reaction temperature and solvent composition also affected the kinetics of precipitation, size, morphology and monodispersity of the spherical particles. With the aid of a microfluidic flow reactor,[106–108] Ogawa and co-workers recently fabricated monodisperse titania-octadecylamine hybrid sub-micrometer-sized spheres using a discrete sol-gel hydrolysis and self-assembly processes. In this synthesis, pre-hydrolyzed amorphous titania primary colloids prepared within a Y-type flow reactor were subsequently assembled into spherical particles in a batch reactor in the presence of octadecylamine as a structure-directing agent (**Figure 5**). Adjusting the flow speed, the hydrolysis and condensation of titanium (IV) isopropoxide and residence time of the titania primary colloids within the flow reactor can be readily controlled, and thus result in the formation of titania-octadecylamine hybrid spheres with variable monodispersity in size. A fast flow (2.5 to 40 mL min^{-1}) gave rise to the spheres with a narrow particle size distribution (coefficient of variation, CV, of 4–7%), while slow flow (0.5 mL min^{-1}) gave rise to polydisperse spheres with a CV of 27%. Octadecylamine plays a vital role in controlling the formation of spherical particles (Figure 5). Irregular particles formed in the absence of octadecylamine and the diameter of the titania-octadecylamine hybrid spheres decreased from 890 to 470 nm when the octadecylamine to titanium (IV) isopropoxide mole ratios were increased from 0.06 to 0.18. Washing with an HCl-ethanol mixed solvent, removed octadecylamine from the hybrid spheres when the mole ratio of octadecylamine/titania oxide was less than 0.25 and produced nanoporous amorphous titania spheres with a specific surface area of 620 m^2 g^{-1} and a uniform pore size centered at 2.2 nm.

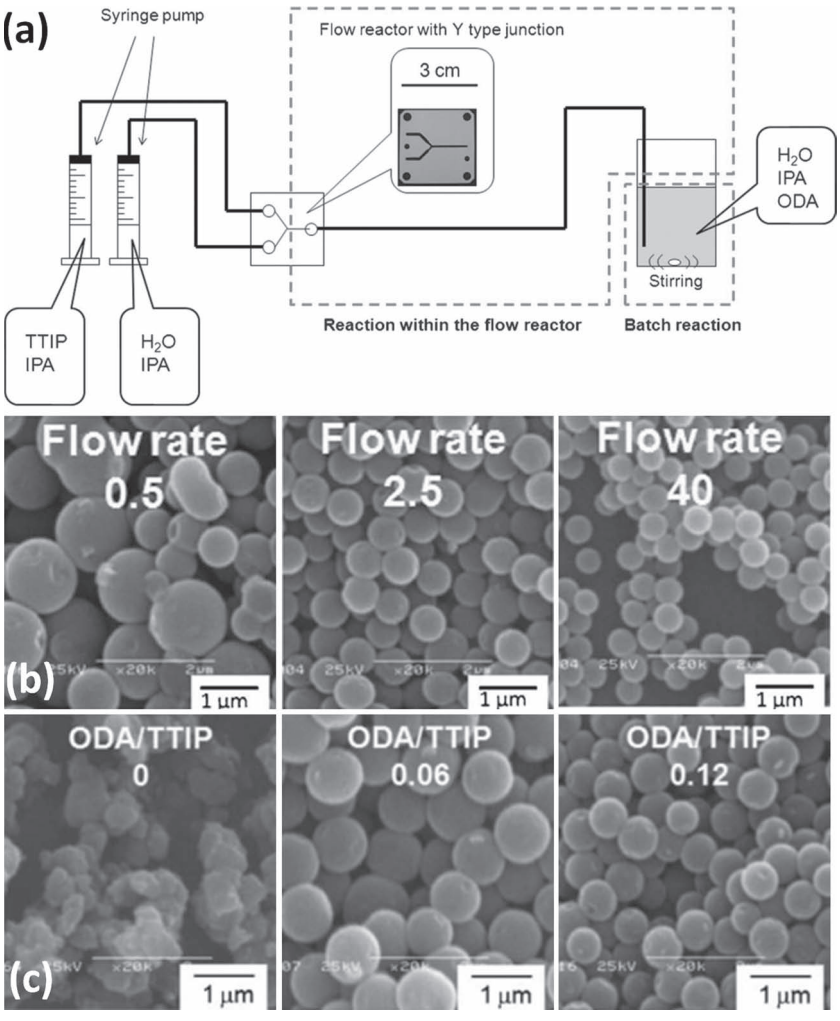

Figure 5. a) Schematic of the sol-gel synthesis of titania microspheres using a flow reactor. b) SEM images of the titania microspheres prepared with varied flow rates (from 0.5 to 40 mL min^{-1}). c) SEM images of the titania microspheres prepared with different ODA:TTIP molar ratios (from 0 to 0.12, ODA: Octadecylamine). Adapted with permission.[108] Copyright 2012, Royal Society of Chemistry.

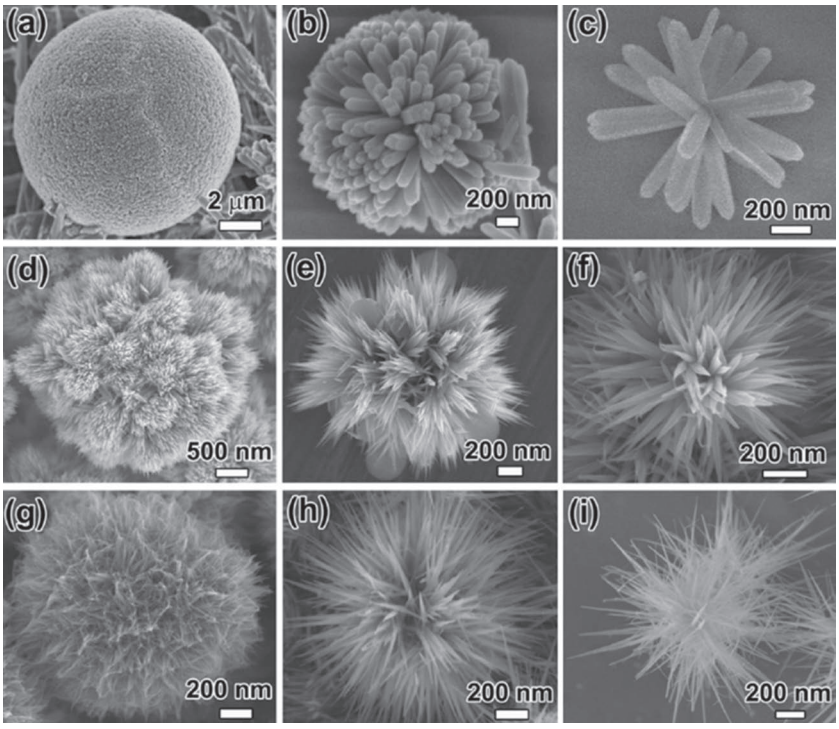

Figure 6. SEM images of the dendritic rutile nanostructures: a–c) Spherical assemblies consisting of nanorod subunits obtained from aqueous titanium (IV) isopropoxide solutions with continuously reduced titanium (IV) isopropoxide concentrations (from a to c). d–f) Spherical assemblies consisting of nanoribbon subunits obtained from mixed aqueous titanium (IV) isopropoxide and ethylene glycol solutions with continuously increased ethylene glycol amounts (from d to f). g–i) Spherical assemblies consisting of nanowire subunits prepared in the presence of 5 mmol urea from mixed aqueous titanium (IV) isopropoxide and ethylene glycol solutions with continuously increased ethylene glycol amounts (from g to i). Reproduced with permission.[110] Copyright 2011, American Chemical Society.

2.6. Hydrothermal/Solvothermal Method

As a versatile method to synthesize diverse, well-dispersed nanocrystals, the hydrothermal/solvothermal process has been employed to prepare spherical titania nanostructures with well-defined morphologies.[109–125] Recently, spherical 3D dendritic titania nanostructures consisting of rutile nanorods, nanoribbons or nanowire subunits have been fabricated via hydrolysis and controlled crystallization of titanium (IV) isopropoxide in the presence of cetyltrimethyl ammonium bromide and HCl (**Figure 6**).[110] The morphologies of the constituent units can be readily changed from nanorod to nanoribbon and nanowire by adding ethylene glycol and urea during the hydrolysis and crystallization step. The diameters and specific surface areas of the dendritic titania nanostructure can be tuned from 1.3 to 10 μm and 25 to 97 m^2 g^{-1}, respectively, by varying synthesis conditions including concentrations of the titanium (IV) isopropoxide, cetyltrimethyl ammonium bromide, ethylene glycol and urea. Kuang and co-workers prepared hierarchical anatase titania microspheres consisting of nanorods and nanoparticles via a hydrothermal process in an acetic acid solution combined with a thermal treatment.[46] Hydrothermal treatment at 140 °C in the presence of acetic acid formed ≈2.1 μm hierarchical Ti-complex intermediate ($Ti_6O_6(Ac)_6(OBu)_{6-n}(OH)_n$, $0 \le n \le 6$) microspheres consisting of nanoribbons. These intermediate microspheres can be readily converted into anatase titania microspheres composed of nanorods and nanoparticles without obvious shrinkage in particle diameter after thermal treatment at 500 °C. Zhao and co-workers reported the synthesis of anatase titania microspheres with exposed mirror-like plane {001} facets derived from hydrothermal crystallization.[109] To synthesize such unique microspheres, Ti foils were first dissolved in a dilute HF solution (0.5 vol%), then sealed in an autoclave and heated to 180 °C for 3 h. The resultant titania microspheres had diameters ranging from 1.5 to 2.1 μm, and the surface of these microspheres was covered by square-shaped {001} crystalline facets. These titania microspheres show an enhanced light scattering capability when used as a scattering layer in dye-sensitized solar cells.

The diverse properties of organic solvents give the ability to tune the morphologies and textures of the resulting titania materials during the solvothermal process.[57,116–124] For example, diluting titanium (IV) isopropoxide in isopropyl alcohol and adding diethylenetriamine, Lou and co-workers fabricated spherical assemblies of anatase flakes with nearly 100% exposed {001} facets via a solvothermal treatment at 200 °C for 24 h.[57] The spherical flaky assemblies had an average size of 1 μm and a specific surface area of 170 m^2 g^{-1}. This morphology imparted the materials with excellent properties for fast reversible lithium storage due to the extremely short transport length scales in the [001] direction and the pores facilitated fast lithium insertion/extraction. Hierarchically porous spherical titania nanostructures composed of anatase ultrathin nanosheets (≈7 nm in thickness) were obtained via a solvothermal process using titanium tetrafluoride as the precursor and diethylene glycol as the reaction medium in the presence of acetic acid.[121] The constituent anatase nanosheets have over 90% high energy {001} facets exposed due to the presence of fluorine species during the solvothermal synthesis. The fluorine species can be removed by a thermal treatment at 600 °C in air. The diameter of the spherical structures decreased from ≈250 nm to ≈200 nm by increasing the concentration of the titanium tetrafluoride from 10 mM to 30 mM. Meanwhile, the quantity of the constituent anatase nanosheets in the products tended to increase without an obvious increase in the thickness of the nanosheets. The product had a specific surface area of 63.5 m^2 g^{-1}, and bimodal mesopores centered at 2.5 nm and 17.9 nm. Bian and co-workers synthesized spherical anatase aggregates with single crystal-like properties and preferable exposure of {001} facets via a solvothermal process using $TiOSO_4$, dilute sulphuric acid and *tert*-butyl alcohol.[126] These titania aggregates were constructed by oriented attachment of primary anatase nanocrystals along their (101) planes during solvothermal crystallization. Selective

and effective adsorption of SO_4^{2-} on the (001) planes of the primary anatase nanocrystals enabled the preferential exposure of such highly active planes. As evidenced by elemental analysis, the sulphate species could be completely removed by washing. The resulting materials possessed a high surface area of 180 m^2 g^{-1} and a disordered mesopore centered at 3.4 nm. Nitrogen-doped mesoporous titania microspheres were fabricated by reacting titanium (IV) butoxide and urea in a HCl-ethanol mixture at 130 °C for 6 h within an autoclave, followed by a thermal treatment at 400 °C for 2 h.[119] The urea played a crucial role in the product formation: Increasing the urea:Ti mole ratio from 0 to 3 during the solvothermal reaction process increased the specific surface area and pore size of the final products from 101 to 154 m^2 g^{-1} and 3.8 to 6.6 nm, respectively, whereas the uniformity of the spherical morphology decreased. The nitrogen content of the calcined microspheres increased slightly from 0.50 to 0.81 at% when the initial urea:Ti mole ratio increased from 1 to 3. The nitrogen-doped mesoporous titania microspheres showed higher visible-light photocatalytic activity than the undoped counterparts.

2.7. Combined Sol-Gel Self-Assembly and Solvothermal Process

Due to the high reactivity of the titanium dioxide precursors and the complexity of the synthetic procedures, there is no facile process reported on the synthesis of titania spheres that simultaneously controls a number of properties: including high specific surface area, variable pore size, high crystallinity, monodisperse particle size and well-defined spherical morphology. This can be achieved by combining sol-gel chemistry with a solvothermal process as illustrated in **Figure 7**.[38–45] The morphology, monodispersity in size and diameter of the mesostructured hybrid beads can be controlled during the sol-gel cooperative self-assembly process in the presence of a structure-directing agent (e.g., hexadecylamine, HDA), whereas crystallite size, specific surface area, and pore size distribution of the anatase titania beads can be varied by altering the ammonia concentration in a solvothermal process or the temperature of solvothermal crystallization and calcination.

Typical structures of the amorphous precursor beads and resultant mesoporous titania (anatase) beads are shown in **Figure 8**.[39,40] Monodisperse hybrid precursor beads with tunable diameter were produced during the sol-gel synthesis (Figure 8a–c). The diameters of the precursor beads can be tuned from 300 to 1150 nm by varying the H_2O:Ti mole ratios from 10:1 to 3:1. These hybrid precursor beads possess a fairly smooth surface and uniform wormhole-like mesostructure throughout the whole bead. They also have quite low specific surface areas and pore volumes due to the presence of HDA in the interstices among the primary sol particles. The precursor beads are amorphous as revealed by the XRD studies. To prepare mesoporous titania beads with a highly crystalline framework and controllable mesoporosity, a solvothermal treatment was conducted in the presence of ammonia. As shown in Figure 8d, monodisperse mesoporous titania beads were obtained after this solvothermal treatment and calcination in air. The beads had rough granular surface features and were composed of anatase nanocrystals with a size < 18 nm (Figure 8e). Increasing the concentration of ammonia used in the solvothermal treatment leads to an [010] direction oriented growth of the anatase nanocrystals and results in the formation of elongated nanoparticles (Figure 8f). Abundant mesopores were found throughout the spherical anatase particle (Figure 8g), and a well interconnected and densely packed nanocrystal network was observed within the titania beads (Figure 8h).[38] As revealed by the corresponding HRTEM image shown in Figure 8i, intergrowth between the anatase crystals occurred during the solvothermal process.

Using a similar synthesis strategy, Yoon and co-workers recently investigated the effects of carbon chain length of the n-alkylamine and sol-gel synthesis temperature on the monodispersity and particle diameter of the amorphous precursor beads.[127] To avoid hydrolysis of titanium (IV) isopropoxide prior to the sol-gel synthesis of the precursor beads, the synthesis was conducted under an inert argon atmosphere using pre-distilled titanium (IV) isopropoxide and ethanol. The monodispersity of the resulting amorphous precursor beads was improved by removing the pre-existing nuclei in the as received titanium (IV) isopropoxide and employing n-alkylamines containing 10, 12, or 14 carbon atoms in the alkyl chain. Upon such optimization, monodisperse amorphous precursor beads with a relatively low standard deviation (less than 4%) in particle size were successfully fabricated at synthesis temperatures ranging from 0 to −20 °C, and the diameter of the resulting precursor beads increased from 900 to 2040 nm over this

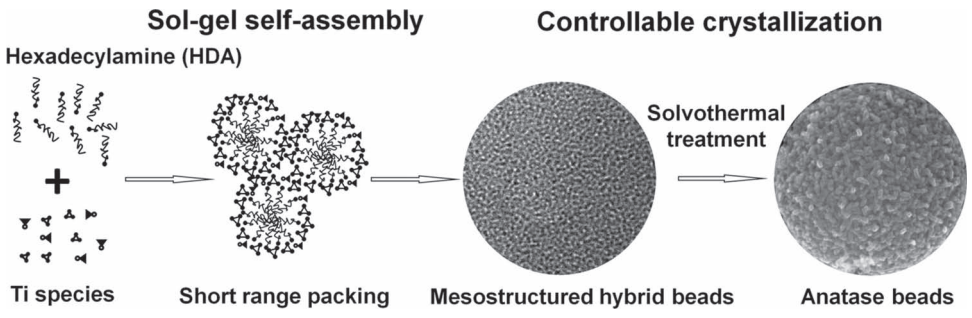

Figure 7. Schematic illustration of the synthesis of monodisperse mesoporous titania beads using a combined sol-gel self-assembly and solvothermal process. Adapted with permission.[40] Copyright 2010, American Chemical Society.

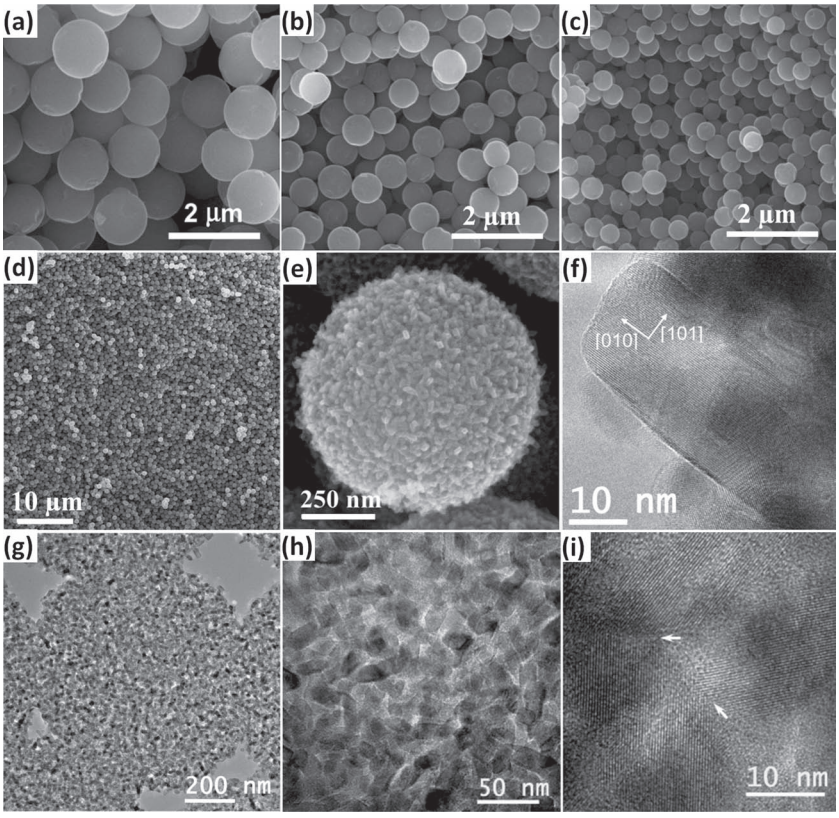

Figure 8. SEM images of the monodisperse amorphous precursor beads of tunable diameters prepared with H_2O:Ti mole ratio of a) 3:1, b) 5:1 and c) 7:1. SEM images of the d) monodisperse mesoporous anatase beads and e) at higher magnification showing the rough granular surface features and the presence of elongated nanocrystals. f) TEM image of the elongated nanocrystal revealing that anatase crystal grows along the [010] direction and increases the abundance of (101) plane. g,h) TEM images of an ultramicrotomed section of the titania beads showing abundant mesopores throughout the anatase titania beads, well interconnected and densely packed nanocrystal networks within the titania beads, and i) intergrowth between titania nanocrystals. Panels (a,b,e,f) reproduced with permission.[40] Copyright 2010, American Chemical Society. Panels (g–i) reproduced with permission.[38] Copyright 2010, American Chemical Society.

temperature range. After solvothermal treatment and calcination, the pore diameters of the resulting mesoporous titania beads can be increased from 5 to 13 nm by doubling the carbon chain length of the n-alkylamine from 8 to 16, along with an increase in the corresponding pore volumes from 0.12 to 0.41 $cm^3\ g^{-1}$. This combined sol-gel self-assembly and solvothermal synthesis strategy has recently been demonstrated as a versatile procedure to fabricate mesoporous anatase beads with variable composition, porosity and surface properties for diverse applications.[47,127–143]

2.8. Other Synthesis Methods

Spherical anatase single crystals less than 30 nm in diameter have been successfully fabricated using a CO_2 laser vaporization method.[144] Continuous radiation of 2 kW laser power yielded ≈21 nm anatase nanoparticles (with a specific surface area of 40.9 $m^2\ g^{-1}$) at a production rate of 16.9 g titania powder per hour, while the use of pulsed radiation of 170 W mean laser power resulted in ≈16 nm anatase nanocrystals (with a specific surface area of 58.9 $m^2\ g^{-1}$) at a reduced production rate of 1.3 g titania per hour. Using the well-established flame pyrolysis process, isolated spherical titania nanoparticles with a particle size ranging from 10 to 100 nm have been prepared using titanium (IV) isopropoxide as the precursor.[145] Both precursor concentration and flame temperature play important roles in controlling the average particle size and morphology. High precursor concentration and low flame temperature can promote precipitation within the precursor droplets and thus result in relatively large spherical titania particles. Kim and co-workers synthesized micrometer-sized amorphous titania spheres by forced hydrolysis of 0.1 M titanium tetrachloride in a mixed solvent of 1-propanol and water at 70 °C.[146,147] Adjusting the volume ratio of 1-propanol to water in the mixed solvent, the dielectric constant and zeta potential of the solvent can be varied and thus results in the precipitation of amorphous titania particles with different morphologies. Discrete spherical titania particles formed when the volume ratio of 1-propanol to water was 3. Adding a small amount (0.64 mg mL^{-1}) of hydroxypropyl cellulose (as a steric dispersant) in the precursor solution produced well-dispersed spherical titania particles with a narrow size distribution. By hydrolyzing a 0.015 M titanium (III) chloride aqueous solution containing 0.5 M urea at 70 °C for 2 h,[148] Ishigaki and co-workers fabricated ≈150 nm spherical titania assemblies consisting of ≈25 nm brookite nanocrystals with a specific surface area of 41 $m^2\ g^{-1}$. These assemblies remained in the brookite phase when heated at 500 °C for 2 h and were converted to rutile on heating at 700 °C for 2 h, along with a significant decrease in the surface area to 9.7 $m^2\ g^{-1}$. Maier and co-workers prepared spherical $TiO_2/CdSO_4$ composites by hydrolyzing acetylacetone stabilized titanium (IV) butoxide in the presence of cadmium acetate dehydrate, thiourea, 1-thioglycerol and *N,N*-dimethylformamide:water (3:1 volume ratio) solvent.[55,56] Etching away the $CdSO_4$ in the composite with 10 wt% HNO_3 aqueous solution gave ≈300 nm mesoporous anatase spheres with a high surface area of 130 $m^2\ g^{-1}$ and a broad pore size distribution ranging from 3.2 to 33 nm. Using a rapid microwave treatment heating at 150 °C for 10 min, mesoporous anatase titania microspheres with a diameter ranging from 150 to 250 nm were prepared using spherical titanium glycolate precursors derived from an ethylene glycol mediated sol-gel synthesis.[149] Through a facile and inexpensive colloidal route, Pagnoux and co-workers fabricated millimeter sized titania beads by granulating commercial anatase powders dispersed in aqueous solution in the presence of polyelectrolytes such as poly(sodium 4-styrenesulfonate) and chitosan (a polycation).[150–152]

3. Applications

As mentioned in the introduction and briefly alluded to in the above synthesis section, the spherical titania nanostructures have been applied in a range of applications. Below we have segmented the examples based on chromatography, energy-storage and conversion, light induced chemistry, electrorheology, catalysis and then applications that do not fit into these categories.

3.1. Packing Materials for Chromatographic Separation

3.1.1. High-Performance Liquid Chromatography (HPLC)

Compared to silica (the most widely used packing material for HPLC), titania shows superior chemical and pH stability, and different surface properties, which makes titania a highly promising support material for HPLC applications under rigorous analytical conditions.[11–13] For this purpose, significant effort has been devoted to the fabrication of titania sorbents with controllable particle size, porosity and crystallinity. Moreover, to achieve mechanically stable packing beds and reduce the pressure drop over the column, micrometer-sized spherical titania particles with a narrow size distribution are highly desirable.[11,13,48,153] Zuo and co-workers reported the synthesis of titania microspheres with a particle size of 3.5 ± 0.5 μm using a polymerization induced colloid aggregation method.[153] The calcined titania microspheres had a surface area of 36.7 m^2 g^{-1} and an average pore diameter of 32.2 nm. Recently, HPLC grade titania microspheres for normal phase chromatography have become commercially available (Sachtopore, made by Sachtleben, Duisburg, Germany),[48] with fairly monodisperse particle sizes (ranging from 3 to 80 μm) and a narrow pore diameter of 6, 10, or 30 nm in the anatase phase. For the rutile phase, the corresponding packing materials have a pore diameter up to 200 nm. These Sachtopore titania packing materials are stable against acid and base, and therefore extend the HPLC separation towards more rigorous analytical conditions. Furthermore, the homogeneous surface properties of such titania packing materials result in high selectivity for a large variety of diverse sorbates of interest. In addition, the slightly acidic surface of the titania packing materials enables the separation of basic molecules (e.g., diverse amines) using a nonfunctionalized titania column (**Figure 9**).

3.1.2. Selective Enrichment of Phosphopeptides

Titania microspheres also show promise towards the selective enrichment of phosphopeptides from proteolytic digests due to the high affinity of titania to the phosphate ions, its high stability in an acidic environment, and its tolerance of most buffers used in biological experiments.[49–51,154–156] Heck and co-workers reported an automated online liquid chromatographic approach to selectively enrich phosphopeptides from proteolytic digests using a titania microcolumn (100 μm internal diameter and 10 mm in length) packed using ≈5 μm microspheres (Titansphere, GL Science Inc., Tokyo, Japan).[49] These titania chromatographic microcolumns manifest a strong affinity and an efficient isolation of the phosphorylated peptides at femtomole level with a high recovery, about 90%, indicating a high potential in the field of quantitative phospho-proteomics. An offline approach employing a titania chromatographic microcolumn prepacked within a pipette tip was also developed to isolate and enrich phosphorylated peptides for proteomics research.[50,51]

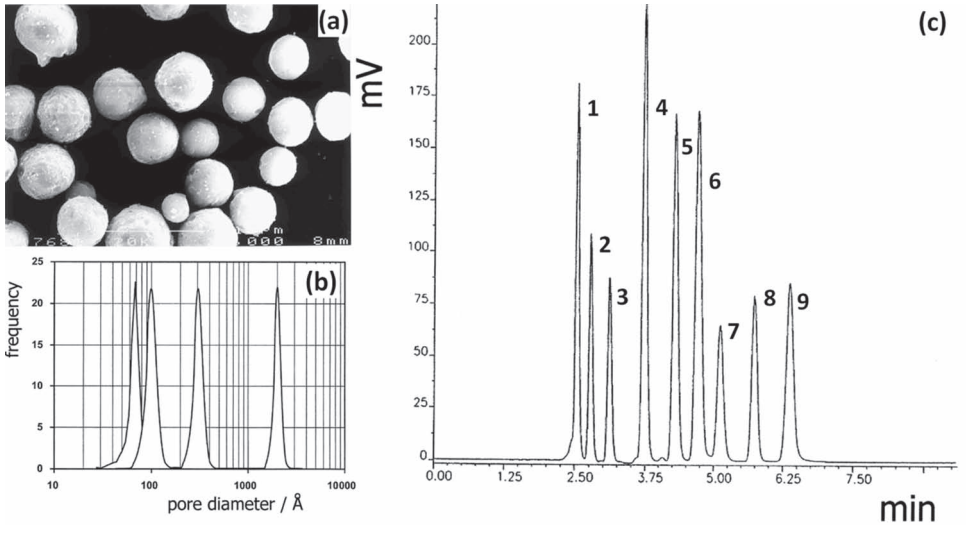

Figure 9. a) SEM image of the Sachtopore titania beads with an average diameter of 5 μm. b) Typical pore diameter distributions of the Sachtopore titania beads (6, 10, 30, or 200 nm). c) Separation of substituted aniline and pyridine derivatives on native titania: 1) *N*,*N*-Dimethylaniline, 2) 2-ethylaniline, 3) *N*-methylaniline, 4) 2,6-dimethylpyridine, 5) 2-methylpyridine, 6) 2,4-dimethylpyridine, 7) pyridine, 8) 4-methylpyridine, 9) aniline. Sorbent: native 5 μm titania beads with 10 nm mesopores. Column: 150 mm × 4 mm. Eluent: n-heptane–2-propanol (99.5:0.5, v:v). Flow: 0.75 cm min^{-1}. Detection: UV at 254 nm. Temperature: ambient. Pressure: 16 bar. Reproduced (panel a) and adapted (panel b and c) with permission.[48] Copyright 2000, Elsevier Science B. V.

Selective enrichment and overall recovery of the phosphopeptides from complex biological mixtures (e.g., human SKBr3 breast cancer cells) can be substantially improved by adding glutamic acid in the sample loading buffer to reduce nonspecific binding of nonphosphorylated peptides to the titania.[157] This offline approach has also been demonstrated as a simple and universal protocol for phosphopeptide purification and was well suited for the characterization of phosphoproteins from both in vitro and in vivo studies in combination with mass spectrometry. Such chromatographic microcolumns packed using titania beads within the pipette tip are commercially available (e.g., Phos-TiO Kits, GL Sciences, Japan, or Toptip Columns, Glygen, Columbia).

Another simple protocol to selectively isolate phosphopeptide was achieved by directly adding titania beads to the protein digests. In this case, the ratio between titania beads and loaded peptides can be readily adjusted to optimize the phosphoproteome selectivity.[158] Zhang and co-workers prepared ≈1 μm mesoporous anatase beads using a combined sol-gel and solvothermal process in the presence of ammonia solution.[155] Due to the high surface area of 85 m^2 g^{-1} and relatively large mesopores centered at ≈18 nm, these mesoporous anatase beads showed a much higher binding capacity for phosphate groups and thus a much higher isolation efficiency for phosphopeptides from digests of the rat brain tissue extract, as compared with non-porous counterparts and commercial titania nanopowders. Yin and co-workers employed sub-micrometer-sized titania colloidal spheres to selectively enrich phosphopeptides from the digests of standard phosphoproteins and complex samples.[52,53] The spheres could be well-dispersed in solution of the digests for adsorption and then easily separated via centrifugation, and have demonstrated a high adsorption capacity and high selectivity towards the enrichment of phosphopeptides. By incorporating superparamagnetic iron oxide nanocrystals into the spheres, separation of titania colloidal spheres from the analyte solution can be simplified by using a magnet.

3.2. Lithium Ion Batteries

Due to numerous appealing features, such as excellent rate capability, high safety, being environmentally benign, and of low cost,[54–57,159–162] titania has attracted extensive interest as a potential anode material for high performance lithium ion batteries. Various titania polymorphs (anatase, rutile and TiO_2-B) and nanostructured morphologies have been applied as anodes in recent years.[54,159,160] Among the various morphologies of the titania nanostructures, spherical particles are highly desired because of their good mobility and high packing density, which is beneficial for the fabrication of uniform and close-packed particulate networks in the electrode,[54–57] thus imparting enhanced volumetric energy density and rate capability to the batteries.

Spherical flaky assemblies of anatase nanosheets with exposed {001} facets, an average size of 1 μm and specific surface area of 170 m^2 g^{-1} were employed as the anode materials in lithium ion battery studies.[57] This resulted in a reversible capacity of 174 mAh g^{-1} at 1 C rate (170 mA g^{-1}), and 136 mAh g^{-1} at 5 C (850 mA g^{-1}) after 100 charge-discharge cycles. Even with a current density up to 20 C (3400 mA g^{-1}), a reversible capacity of 95 mAh g^{-1} was obtained, indicating a remarkable rate capability for the resulting materials. The unique flaky anatase nanostructures gave an extremely short transport length in the [001] direction of anatase for lithium insertion/extraction, and thus the excellent rate performance. After 100 charge-discharge cycles at 5 C, the overall spherical morphology of the particles and the long-range ordered anatase crystal phase were retained, indicating good structural stability of the resulting materials. The TiO_2-B (bronze) phase has a much higher theoretical capacity (335 mAh g^{-1}), hence Liu and co-workers fabricated mesoporous TiO_2-B microspheres (ca. 1 μm in diameter) via a combined colloidal silica templating and aerosol-assisted pyrolysis process.[54] These TiO_2-B microspheres displayed superior rate performance with 165 mAh g^{-1} at 10 C (3350 mA g^{-1}), 130 mAh g^{-1} at 30 C (10 050 mA g^{-1}) and 116 mAh g^{-1} at 60 C (20 100 mA g^{-1}), whereas the commercial titania (anatase) nanoparticles of similar surface area (123 m^2 g^{-1}) only obtain 70 mAh g^{-1} at 10 C, 36 mAh g^{-1} at 30 C and 23 mAh g^{-1} at 60 C (**Figure 10**). After 5000 charge-discharge cycles at relatively high (10 C) current rate, the capacity of the TiO_2-B microspheres was maintained at 149 mAh g^{-1} (only 10% capacity loss compared with the starting capacity of 166 mAh g^{-1}), indicating the excellent cyclability of these TiO_2-B microspheres (Figure 10). The superior rate capacity and cyclability was ascribed to the following integrated features: 1) fast pseudocapacitive reaction involved on the surface of the materials; 2) adequate electrode-electrolyte contact due to the well-connected mesoporosity (uniform 12 nm mesopores) and relatively high surface area (126 m^2 g^{-1}); 3) compact particle packing density in the electrode layer; and 4) excellent structure stability that results in negligible volume/strain changes of the nanostructures during the lithium insertion/extraction process.

3.3. Dye-Sensitized Solar Cells (DSCs)

Spherically shaped anatase particles with high specific surface area and large mesopores have demonstrated high promise for use in working electrodes for DSCs.[38–47,89,91,92,131,132,135,140,141] Monodisperse mesoporous anatase beads with variable surface area, pore diameter and particle size prepared using a combined sol-gel self-assembly and solvothermal process have been applied as titania electrodes with diverse configurations for DSCs.[38–45]

3.3.1. Single Layered Titania Bead Films

A high solar to electric power conversion efficiency (PCE) of 10.6% was achieved (**Figure 11**a) on a 12 μm thick anatase bead film on FTO glass after sensitization using C101, a Ru(II)-based dye.[38] As revealed by the corresponding incident photon to current conversion efficiency (IPCE) curves, anatase bead electrodes manifest a superior performance to those made from the titania nanocrystals (Degauss P25) over the entire range of spectrum in which the C101 dye absorbs effectively (Figure 11b). The normalized IPCE curves (Figure 11c) show the bead electrodes had enhanced photon conversion efficiency at relatively long wavelengths (from 600 to 800 nm). This improved light

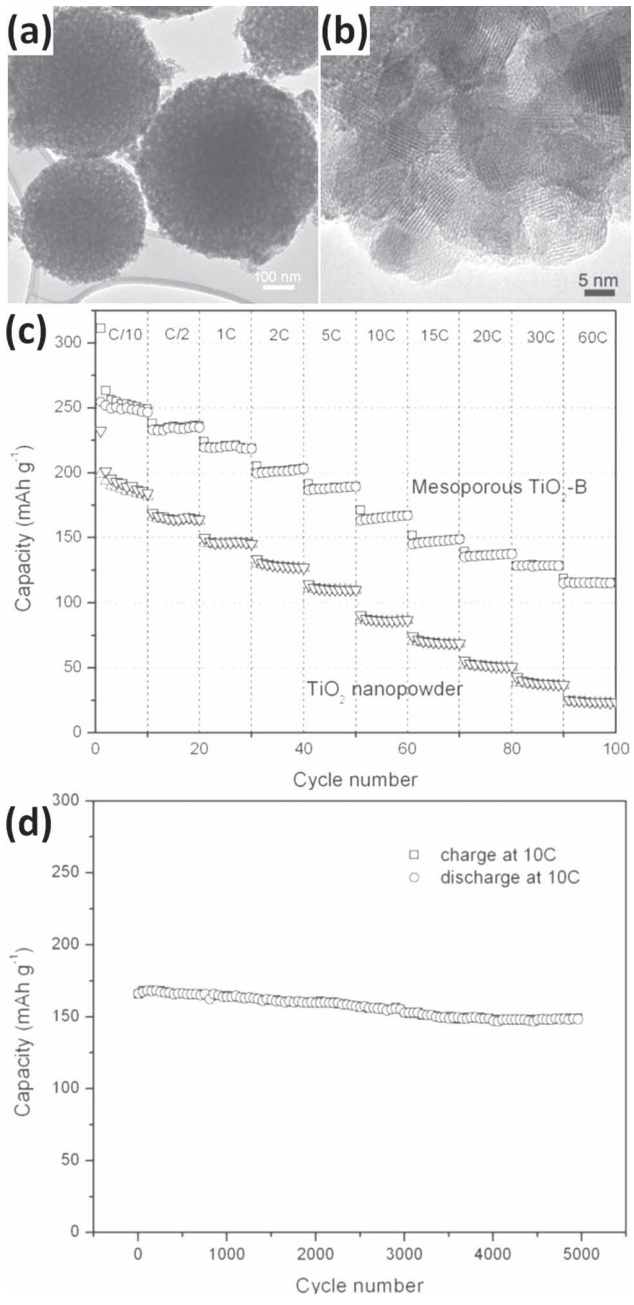

Figure 10. a) TEM and b) HRTEM images of the mesoporous TiO_2-B microspheres (ca. 1 μm in diameter). c) Rate performance of the mesoporous TiO_2-B microspheres and a commercial anatase nanoparticle electrode at different C rates (1 C = 335 mA g^{-1}). d) Cycling performance of the mesoporous TiO_2-B microspheres during 5000 charge-discharge cycles at a high current rate of 10 C (3350 mA g^{-1}). Reproduced with permission.[54]

conversion characteristic originates from a combination of the increased dye loading of the bead electrodes (due to the high surface area of the beads) and higher diffuse reflectance (due to the bead morphology and size) in the visible and near-infrared regions from 450 to 800 nm (Figure 11d).[38,39,42,45,47,132] The enhanced optical features could increase the pathlength of the photons within the titania bead electrodes due to scattering, and thus improve the light harvesting and conversion efficiencies.[38,39,42,163,164] Moreover, the well interconnected and densely packed nanocrystal network within the titania beads (Figure 8g,h), along with the enhanced chemical bonding (intergrowths) between anatase nanocrystals (Figure 8i), promote the passing of electrons through the titania grain boundaries.[38] Thus extending the electron lifetime and diffusion length within the bead electrodes[38,46,47] (Figure 11e,f).

3.3.2. Scattering Layer

To reduce possible photon loss (incident light that generally transmits through the film), a bi-layered electrode was constructed with an upper scattering layer composed of porous titania beads.[42,47,109,129,132,140] A 6 μm thick titania (CCIC, 18 nm) nanocrystalline film was deposited on FTO glass and then anatase bead films of 6 or 11 μm thickness placed on top.[42] Due to the relatively large bead size and high surface area of the mesoporous anatase beads, this upper layer served as a scattering layer and contributed to the electrode function. The PCE was improved by 42.8% with an 11 μm thick mesoporous bead film on the anatase nanocrystal film.[42] Further optimization of the stacking structures of the titania electrodes included a triple layered electrode,[38] consisting of a layer of 20 nm anatase nanocrystals, then a layer of mesoporous titania beads and a top layer of CCIC-400 nm scattering particles. A PCE of 11.2% (open circuit photovoltage of 725 mV, short circuit photocurrent of 19.9 mA cm^{-2} and fill factor of 0.77) was achieved using this triple layered titania electrode after sensitization using C106, a Ru(II)-based dye.[38]

3.3.3. Flexible DSCs

Flexible DSCs constructed on conductive plastic substrates have gained lots of attention recently.[43,44,165,166] To improve the PCE of the flexible DSCs, porous titania films with improved contacts between the titania nanocrystals are required to ensure efficient electron transport across particle boundaries. Well-crystallized anatase beads with high surface area (61 m^2 g^{-1}) were fabricated by pre-sintering the solvothermally-treated titania beads at relatively high temperature (e.g., 650 °C) to enhance chemical bonding between neighbouring nanocrystals within the spherical assemblies.[44] When these pre-sintered mesoporous titania beads were used to fabricate the flexible DSCs via a cold isostatic pressing method, an impressive PCE of 6.59% was achieved. In contrast, a PCE of 4.94% was recorded on the flexible DSCs made from the conventional anatase nanocrystals. The electron diffusion coefficient of the cells employing pre-sintered anatase bead films was about an order of magnitude higher than that of the titania nanocrystal electrodes. Treating the pre-sintered mesoporous beads with dilute $TiCl_4$ aqueous solution improved the PCE of the resulting flexible DSCs to 7.54%, clearly indicating great promise of such anatase beads as candidates for high performance flexible DSCs. In general, such mesoporous anatase beads can be purposely pre-treated (e.g., pre-sensitized with diverse dyes/quantum dots, or pre-coated with various inorganic precursors to achieve core-shell structures) to obtain desirable building blocks for fabricating high efficiency flexible DSCs.[43,44,165,166]

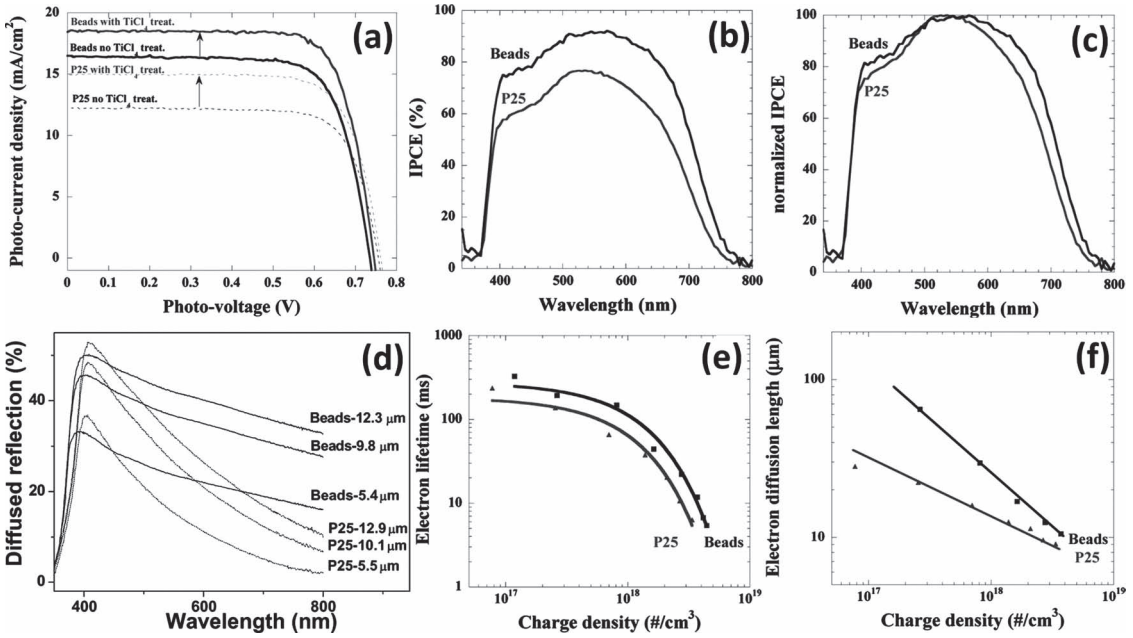

Figure 11. a) *I–V* curves, b) IPCE curves, c) normalized IPCE curves, d) diffuse reflectance spectra, e) electron lifetime and f) electron diffusion length as a function of charge density in titania films made from anatase beads and Degussa P25 nanoparticles. Panels (a–c,e,f) adapted with permission.[38] Copyright 2010, American Chemical Society. Panel (d) reproduced with permission.[39]

3.4. Photocatalysis

Titania has been applied in photocatalytic oxidation processes ranging from the remediation of polluted water and air to H_2 production via water splitting.[20,21] Due to their ease of recovery and efficient charge transfer processes between the nanoparticles within the sphere, spherical titania particles have been widely studied for these applications.[64,81,99,113,133,147]

3.4.1. Photocatalytic Oxidation

Park and co-workers recently prepared graphene-wrapped mesoporous titania (anatase) microspheres and investigated their photocatalytic activities by monitoring the photodegradation of methylene blue, an organic dye, under visible irradiation ($\lambda >$ 420 nm).[133] The spherical graphene-titania composites were fabricated from preformed amorphous titania microspheres.[39,40] The precursor spheres were modified with 3-aminopropyl-trimethoxysilane (APTMS) to obtain positively charged surfaces, then coated with negatively charged graphene oxide nanosheets via electrostatic interactions. The resulting graphene oxide wrapped amorphous microspheres underwent solvothermal treatment in an ethanol-water mixture at 180 °C for 16 h to deoxidate the graphene oxide and crystallize the titania. Calcination at 400 °C for 2 h under an Ar atmosphere was employed to remove the organic components and obtain highly crystalline graphene-wrapped mesoporous anatase microspheres (**Figure 12**). These spheres show an enhanced photocatalytic degradation of methylene blue over the bare anatase microspheres and commercial Degussa P25 nanoparticles (Figure 12). This is due to their extended photon adsorption toward visible light as a result of a reduction in bandgap (from 3.2 to 2.8 eV), and efficient transfer of photogenerated electrons from the excited methylene blue to anatase nanocrystals through the highly conductive graphene nanosheets. Titania microspheres (≈2 μm in diameter) composed of well-crystallized rutile nanorods with exposed reactive {111} facets were hydrothermally synthesized using 0.15 M titanium trichloride solution in the presence of 3 M sodium chloride at 200 °C for 16 h.[167] These rutile microspheres demonstrated excellent photocatalytic antibacterial activity towards *Staphylococcus aureus* as they effectively suppressed photoinduced electron–hole pair recombination and the highly dispersed OH free radicals directly attacked the *Staphylococcus aureus* on the spherical surfaces.

3.4.2. Photocatalytic Water Splitting

Choi and co-workers prepared mesoporous titania (anatase) microspheres with diameters ranging from 0.5 to 1 μm via sol-gel synthesis and calcination at 450 °C for 1 h.[99] The spheres consist of compactly packed anatase nanocrystals (10–15 nm), have a specific surface area of 70 ± 5 m^2 g^{-1} and a mesopore of 3.9 nm. They are highly efficient photocatalysts for H_2 production via water splitting with a fairly low loading (0.1 wt%) of Pt nanoparticles. Under both UV and visible light illumination, such mesoporous anatase microspheres show a superior performance to the synthesized titania colloids, commercial Degussa P25 and Hombikat UV-100. This enhanced effectiveness was ascribed to the well-connected anatase nanocrystal networks within the beads. As revealed by the corresponding photocurrent response curves recorded on the bare titania materials (without Pt loading), this densely packed network was believed to facilitate efficient interparticle charge transfer by retarding the recombination of photoexcited electrons and holes.

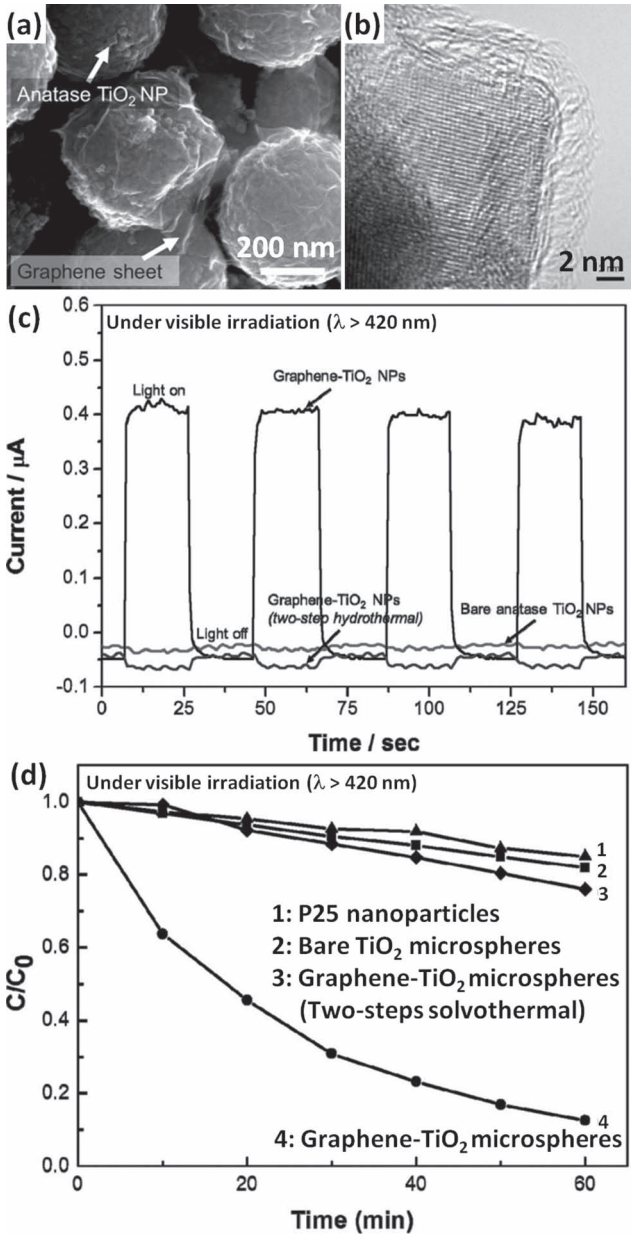

Figure 12. a) SEM image of the graphene-wrapped titania microspheres. b) TEM image showing anatase fringe lattice and graphene layers on the surface. c) Photocurrent responses of the bare titania microsphere, graphene-titania composite and graphene-titania composite (two-step solvothermal) under visible light irradiation ($\lambda > 420$ nm). d) Photodegradation of methylene blue under visible light irradiation and a remarkably enhanced performance of the graphene-wrapped titania microspheres demonstrated by curve 4. Adapted with permission.[133]

3.5. Photoluminescence

Due to its good mechanical, optical and thermal properties, titania has been recognized as a highly promising host material for high efficiency phosphors.[24,82,103,128,134,137,139,168] Ample evidence has demonstrated that efficient host-sensitized luminescence could be realized in trivalent rare-earth ion (RE^{3+})-doped titania materials.[82,103,128,134,137,139,168] To further improve the luminescent performance, definition and screen packing property, non-agglomerated spherical titania particles with a narrow size distribution were required.[103]

Mesoporous spheres of Eu^{3+}-doped titania about 250 nm in diameter were fabricated via a sol-gel synthesis in the presence of a nonionic surfactant.[103] The as-prepared sub-micrometer-sized spheres were amorphous at the atomic scale. After calcination at 400 °C, a titania phosphor material having a surface area of 158 $m^2\ g^{-1}$, pore diameter of 7.6 nm, Eu^{3+} content of 4.95 mol.% and semicrystalline framework was obtained. This material exhibited strong and broad emission lines derived from the excited state of $^5D_0$ to the $^7F_1$, $^7F_2$ and $^7F_3$ states under UV excitation at 360 nm. The semicrystalline frameworks of the 400 °C-calcined titania phosphor is important for efficient luminescence as 1) anatase nanocrystals within the framework act as the sensitizers to transfer the absorbed excitation energy to the Eu^{3+} and 2) glassy amorphous regions within the titania host allow for a well-dispersed Eu^{3+} and thus prevent luminescence quenching from Eu^{3+} aggregation. Using an aerosol-assisted self-assembly method, Wang and co-workers fabricated semicrystalline Eu^{3+}-doped titania microspheres (0.1 to 1.4 μm in diameter) with varying Eu^{3+} contents (3.7 mol% to 14 mol%).[82] After calcination at 400 °C for 4 h in air, the mesoporous titania phosphors had a surface area of 140 $m^2\ g^{-1}$ and a mesopore of 7 nm. Their mesoporous characteristic, which facilitated the distribution of Eu^{3+} within the titania host, allowed high doping contents of up to 14 mol% without observation of luminescence quenching induced by the aggregation of Eu^{3+}. Eu^{3+} and Sm^{3+} co-doped titania microspheres with a total concentration of 12 mol% were also fabricated using this method. In this case, emission peak wavelengths and intensities can be varied by tuning the molar ratio of Eu^{3+} and Sm^{3+}.

For the above semicrystalline titania host materials, RE ions are usually embedded in the amorphous region or the distorted surface sites adjacent to the titania nanocrystals. As a result, only broad and unresolved emission lines of the rare-earth ions could be observed on the resultant phosphors. To obtain sharp, intense and multicolor emission lines of the ions for highly sensitive biolabeling, lighting and display applications, phosphors incorporating RE^{3+} in the lattice of the host materials are in high demand.[24,128,134,137,139] Although considerable effort has been devoted to attain this aim, it remains a challenge due to the large mismatch of the ion radius between RE^{3+} and Ti^{4+} and the charge imbalance. Chen and co-workers recently overcame this issue by developing a combined sol-gel and solvothermal method to fabricate spherical titania phosphors doped with single/dual RE^{3+} (including Eu^{3+}, Sm^{3+}, Er^{3+}, Nd^{3+} and Yb^{3+}) and systematically investigated the electronic structures and optical properties of the resultant phosphors.[24,128,134,137,139] These RE^{3+}-doped titania phosphors were spherical assemblies (around 1 μm in diameter) of 10–20 nm anatase nanocrystals after calcination at 500 °C in air. When Eu^{3+} was used as the dopant, only weak energy transfer from titania host to Eu^{3+} was observed due to the mismatch of energy levels between the titania band-gap and Eu^{3+}.[24] By co-doping Eu^{3+} with Sm^{3+} in the titania host,[128] the energy transfer from titania to Eu^{3+} ions can be greatly enhanced, as the Sm^{3+} is an energy bridge between titania and Eu^{3+}. Using Sm^{3+} or Nd^{3+} as the dopant

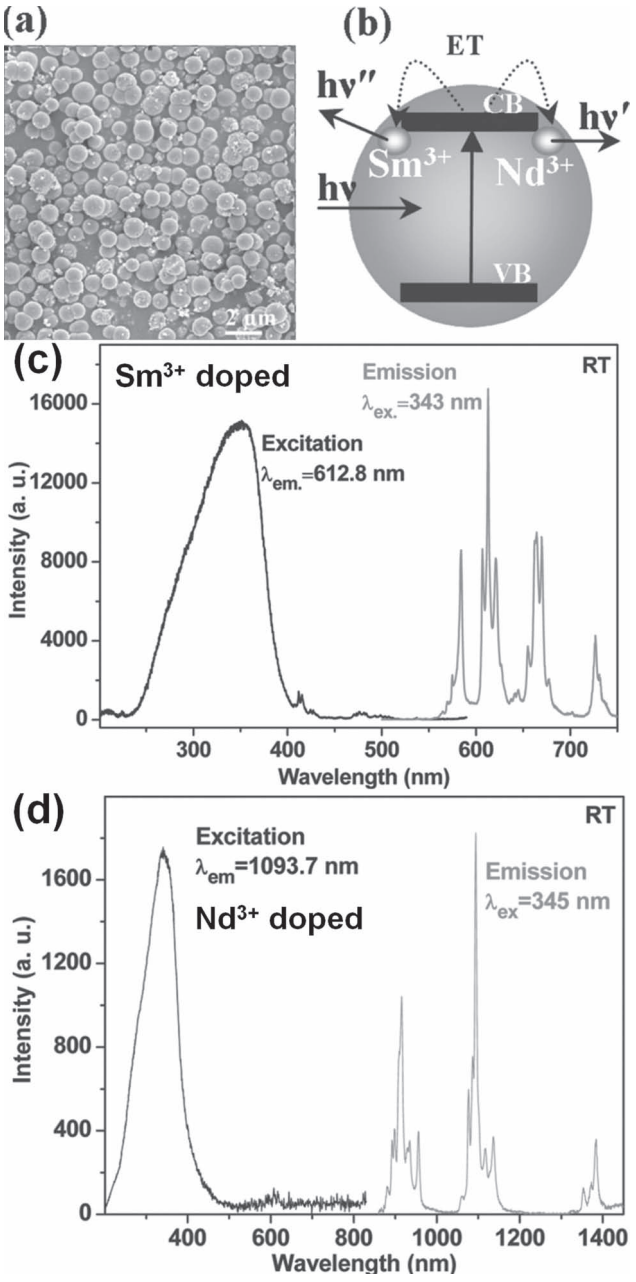

Figure 13. a) SEM image of the spherical Nd^{3+} doped titania phosphors. b) Schematic illustration of the energy transfer (ET) from titania host to Sm^{3+} and Nd^{3+}. c) Excitation (left) and emission (right) spectra of the 2.34 mol% Sm^{3+} doped titania phosphors at room temperature. d) Excitation (left) and emission (right) spectra of the 1.99 mol% Nd^{3+} doped titania phosphors at room temperature. Adapted with permission.[134] Copyright 2009, American Chemical Society.

(**Figure 13**),[134] matching of energy levels between the titania band-gap and Sm^{3+} or Nd^{3+} excited states can be attained, thus intense and resolved emission lines of Sm^{3+} or Nd^{3+} were achieved on the resultant phosphors at relatively low dopant concentrations (2.34 mol% for Sm^{3+} and 1.99 mol% for Nd^{3+}). When Er^{3+} was used as the dopant,[137] titania phosphors with green and red up-conversion luminescence, in addition to the down-conversion luminescence, were achieved upon laser excitation at 974.5 nm. Moreover, intensities of the up-conversion luminescence of the Er^{3+} can be remarkably enhanced (by a factor of about 5 times in green and 6 times in red regions) upon the co-doping of 2.5 mol% Yb^{3+}.[137] This is a result of the efficient sensitization and energy transfer up-conversion process promoted by the Yb^{3+}.

3.6. Electrorheological Fluids

As an environmentally friendly semiconductor with relatively high dielectric constant and polarization ability and low cost for production, titania has been considered as a promising candidate for high performance electrorheological fluids.[169–171] An extremely large yield stress of 200 kPa has been achieved on titania based electrorheological fluids recently.[171] Zhao and co-workers fabricated Cr-doped titania microspheres with hierarchically-structured or relatively smooth surfaces via a combined sol-gel and solvothermal process (150 °C for 72 h), followed by calcination at 600 °C.[170] The hierarchically-structured Cr-doped titania were composed of rutile nanorods with a diameter of 20–30 nm and had a surface area of ≈65 m^2g^{-1} and a mean diameter of 3.2 μm. Contrastingly, the smooth Cr-doped titania microspheres were made from rutile nanocrystals and possessed a relatively low surface area of 5 m^2 g^{-1} and an average diameter of 2.3 μm. Under electric fields the suspension made of the hierarchically-structured Cr-doped titania microspheres possessed a stronger electrorheological effect than those containing smooth Cr-doped titania microspheres due to the improved interfacial polarization and the increased interparticle interaction of the former. This enhanced effectiveness was believed to be associated with the unique surface morphology and relatively high surface area of the hierarchically-structured Cr-doped titania microspheres. Recently, Cheng and co-workers developed an acetic acid modified sol-gel process to prepare monodisperse sub-micrometer-sized titania spheres for electrorheological fluids application.[169] After hydrolysis at 70 °C for 8 h, sub-micrometer-sized anatase spheres with fairly small crystallite size were obtained. The sphere diameters could be tuned from 420, 310 to 240 nm by increasing the mole ratio of acetic acid:titanium (IV) butoxide from 0.4, 1.2 to 3.0, along with an increase in the surface area from 10, 17 to 30 m^2 g^{-1}. The resultant anatase spheres contained polar molecules (e.g., ethylene glycol and acetic acid) on the surfaces of the nanocrystals and the smaller spheres had more polar molecules adsorbed. Rheological experiments revealed that the smaller anatase spheres manifested enhanced electrorheological effects because of the increased polar molecule contents and specific surface area.

3.7. Catalysis

Chen and co-workers fabricated amorphous titania spheres (≈500 nm in diameter) with enriched surface hydroxyl groups (OH-rich titania spheres) by exposing titanium glycolate precursor spheres to UV-light irradiation (400 W high-pressure mercury lamp with main output at 313 nm) for 2 h.[172] These

spheres have a high surface area of 460 m^2 g^{-1}, and a narrow pore diameter centered at 2.3 nm, and they can activate urea under mild conditions (300 °C in air) to form graphitic carbon nitride (a metal-free polymeric photocatalyst). This result demonstrated that carbon nitride materials can be directly prepared using oxygen-containing compounds with the aid of OH-rich titania spheres. Hydroxyl-group-rich spherical titania colloids (≈200 nm in diameter) were also employed as the supports for Pd nanoparticles.[173] Such Pd-loaded titania spheres showed a high catalytic activity for the Suzuki cross-coupling reaction and can be recycled up to five times without any notable loss of catalytic activity due to the firmly-attached and well-dispersed Pd nanoparticles. Using a similar synthesis strategy,[174] Song and co-workers recently fabricated Cu_2O-loaded titania submicrometer-sized spheres and demonstrated their superior catalytic activities towards the Ullmann type cross-coupling reactions between aryl halides and phenol.[174] Such spherical titania catalysts contained well-distributed Cu_2O nanoparticles with enhanced stability on the surfaces and they retained high catalytic activities after five consecutive runs. Titania colloidal spheres, ≈250 nm in diameter, pre-modified with $-NH_2$ groups were loaded with Pt nanoparticles via a facile electrostatic interaction, and the resultant Pt/TiO_2 composites were employed as catalysts for the oxidation of hydrogen peroxide.[175] Due to the great biocompatibility of titania and the excellent catalytic activity of the Pt nanoparticles, such Pt/TiO_2 catalysts exhibited a sensitive and fast detection of glucose with a low detection limit of 0.25 μM, indicating great promise for biosensing application.

3.8. Other Applications

Spherical titania assemblies have also been widely investigated in fields including gas sensors,[115] colloidal photonic crystals,[102,176] heavy metal ion sequestration,[177] and bioimaging and drug delivery.[178] Flower-like titania microspheres composed of radially assembled anatase nanoflakes were prepared via a hydrothermal oxidation of titanium powder in the presence of NaOH and H_2O_2 at 150 °C, and subsequent calcination at 550°C for 2 h.[115] The calcined flower-like titania microspheres were 1 to 1.5 μm in diameter and possessed a surface area of 64.8 m^2 g^{-1}. These hierarchically structured materials showed a sensitivity of 6.4, a response time of 12 s and a recovery time of 9 s when exposed to 100 ppm ethanol vapour. This excellent gas sensing response was believed to be associated with the hierarchical porosity that enables fast diffusion of ethanol gas throughout the titania sensing layer. Monodisperse, sub-micrometer-sized, non-aggregated titania spheres were recognized as promising candidates for colloidal photonic crystals because of their relatively large refractive index and low absorption in the visible and near-infrared regions. Bragg reflections in visible or near infra-red regions were observed on the colloidal photonic crystals made of either 280 or 484 nm titania spheres, respectively.[102,176] Spherical mesoporous titania colloids (≈200 nm in diameter) have demonstrated effective adsorption of As (V) ions from aqueous solution.[177] Wu and co-workers prepared ~350 nm amorphous titania nanospheres via hydrolysis of titanium (IV) ethoxide in ethanol and the resulting titania nanospheres possess a surface area of 237 m^2 g^{-1} and an average mesoscale pore of 2.8 nm.[178] These spheres manifested a good biocompatibility to the human breast cancerous cell line (BT-20) and a LC_{50} (the lethal concentration of 50% cell death) value of 400 mg L^{-1} was determined from the cell viability test. Due to the strong affinity between titania and phosphates, such titania nanospheres can be easily functionalized with diverse phosphate groups containing fluorescent probes for intracellular imaging. The high specific surface area and mesoporosity of the nanospheres gave them a high loading capacity for therapeutic agents (e.g., 21.7 mg g^{-1} for Doxorubicin, a cell membrane impermeable anti-cancer drug) for intracellular drug delivery.

4. Conclusions and Outlook

Advances in the fabrication and application of various spherical titania nanostructures over the last decade have been summarized. A number of important synthesis strategies were detailed including the presence of templates, emulsion-mediated synthesis, aerosol-assisted self-assembly methods, electrospray techniques, sol-gel synthesis, hydrothermal/solvothermal approaches, and a combined sol-gel and solvothermal method. Physical properties of the titania spheres could be controlled depending on the synthesis strategy with variation in polymorph (including amorphous, anatase, rutile, brookite and TiO_2-B), particle size (ranging from tens of nanometer to millimeter scale), specific surface area and porosity, as well as the shape and size of the subunits and surface properties of the products. Due to the characteristics and spherical morphology of these particles they have a relatively high packing density, a high affinity for phosphate ions, excellent structure stability, enhanced light scattering capability, a high dielectric constant and polarization ability, enriched surface hydroxyl groups, excellent biocompatibility, and tunable surface properties. Hence, these spherical titania nanostructures showed excellent performance in applications across numerous fields: biomolecule separation, clean energy utilization, conversion and storage, photoluminescence, electrorheological fluids, catalysis, drug delivery and gas sensing.

Most of the synthesis methods are either a batch procedure or a continuous process with relatively low yield. To achieve widespread utilization of spherical titania nanostructures, a continuous and scalable synthesis method that allows precise control over the physical properties of the material is required. Additionally, as with most colloidal particles, the spherical titania particles, especially those less than 1 μm in diameter, tend to agglomerate as they are separated from solution using centrifugation or filtration and dried. To ensure re-dispersibility or flow of the dried particles, effective drying or storage methods are highly desirable to prevent the formation of irreversible agglomerations. Continued research in this area will extend our understanding of the formation mechanism of these spherical nanostructures and determine key factors of the synthesis process affecting the physical properties. Breakthroughs in scale-up production, collection and storage of spherical titania nanostructures will give rise to practical products employing these versatile titania nanomaterials.

Acknowledgements

The authors would like to acknowledge Dr. Fuzhi Huang and Prof. Yi-Bing Cheng (Monash University), Dr. Frédéric Sauvage, Dr. Pascal Comte, Mr. Leo-Philipp Heiniger and Prof. Michael Grätzel (École Polytechnique Fédérale de Lausanne, EPFL) for their collaboration on the dye-sensitized solar cell projects employing the mesoporous anatase beads. Financial support from the Australian Research Council Discovery Project scheme (DP0985744 & DP110101346) is acknowledged. R.A.C. is the recipient of an Australian Research Council Future Fellowship (FT0990583).

Received: July 7, 2012
Revised: September 12, 2012
Published online: October 18, 2012

[1] J. V. Sanders, *Nature* **1964**, *204*, 1151.
[2] P. J. Darragh, A. J. Gaskin, J. V. Sanders, *Sci. Am.* **1976**, *234*, 84.
[3] F. Caruso, *Colloids and Colloid Assemblies: Synthesis, Modification, Organization and Utilization of Colloid Particles*, Wiley-VCH, Weinheim, Germany **2004**.
[4] X. D. Feng, D. C. Sayle, Z. L. Wang, M. S. Paras, B. Santora, A. C. Sutorik, T. X. T. Sayle, Y. Yang, Y. Ding, X. D. Wang, Y. S. Her, *Science* **2006**, *312*, 1504.
[5] C. W. Sun, S. Rajasekhara, J. B. Goodenough, F. Zhou, *J. Am. Chem. Soc.* **2011**, *133*, 2132.
[6] H. M. Xie, R. S. Wang, J. R. Ying, L. Y. Zhang, A. F. Jalbout, H. Y. Yu, G. L. Yang, X. M. Pan, Z. M. Su, *Adv. Mater.* **2006**, *18*, 2609.
[7] J. R. Ying, C. Y. Jiang, C. R. Wan, *J. Power Sources* **2004**, *129*, 264.
[8] Q. Wang, H. Li, L. Q. Chen, X. J. Huang, *Carbon* **2001**, *39*, 2211.
[9] Q. Wang, H. Li, L. Q. Chen, X. J. Huang, *Solid State Ionics* **2002**, *152*, 43.
[10] S. Q. Wang, Z. D. Lu, D. Wang, C. G. Li, C. H. Chen, Y. D. Yin, *J. Mater. Chem.* **2011**, *21*, 6365.
[11] J. Nawrocki, C. Dunlap, A. McCormick, P. W. Carr, *J. Chromatogr., A* **2004**, *1028*, 1.
[12] J. Nawrocki, C. Dunlap, J. Li, J. Zhao, C. V. McNeff, A. McCormick, P. W. Carr, *J. Chromatogr., A* **2004**, *1028*, 31.
[13] U. Trudinger, G. Muller, K. K. Unger, *J. Chromatogr.* **1990**, *535*, 111.
[14] H. X. Zhang, H. Zhao, J. X. Wang, J. F. Chen, Y. F. Lu, J. Yun, *Small* **2009**, *5*, 1846.
[15] H. X. Zhang, J. X. Wang, L. Shao, J. F. Chen, *Ind. Eng. Chem. Res.* **2010**, *49*, 4156.
[16] M. I. Martinez-Rubio, T. G. Ireland, G. R. Fern, J. Silver, M. J. Snowden, *Langmuir* **2001**, *17*, 7145.
[17] H. Wang, C. K. Lin, X. M. Liu, J. Lin, M. Yu, *Appl. Phys. Lett.* **2005**, *87*, 181907.
[18] A. Weir, P. Westerhoff, L. Fabricius, K. Hristovski, N. von Goetz, *Environ. Sci. Technol.* **2012**, *46*, 2242.
[19] O. Carp, C. L. Huisman, A. Reller, *Prog. Solid State Chem.* **2004**, *32*, 33.
[20] X. B. Chen, S. S. Mao, *Chem. Rev.* **2007**, *107*, 2891.
[21] X. B. Chen, S. H. Shen, L. J. Guo, S. S. Mao, *Chem. Rev.* **2010**, *110*, 6503.
[22] M. Grätzel, *Nature* **2001**, *414*, 338.
[23] A. Fujishima, X. T. Zhang, D. A. Tryk, *Surf. Sci. Rep.* **2008**, *63*, 515.
[24] X. Y. Chen, W. Q. Luo, *J. Nanosci. Nanotechnol.* **2010**, *10*, 1482.
[25] K. Kalyanasundaram, *Dye-Sentitized Solar Cells*, École Polytechnique Fédérale de Lausanne Press, Lausanne **2010**.
[26] M. Wagemaker, A. P. M. Kentgens, F. M. Mulder, *Nature* **2002**, *418*, 397.
[27] X. B. Chen, L. Liu, P. Y. Yu, S. S. Mao, *Science* **2011**, *331*, 746.
[28] D. I. Enache, J. K. Edwards, P. Landon, B. Solsona-Espriu, A. F. Carley, A. A. Herzing, M. Watanabe, C. J. Kiely, D. W. Knight, G. J. Hutchings, *Science* **2006**, *311*, 362.
[29] P. D. Yang, D. Y. Zhao, D. I. Margolese, B. F. Chmelka, G. D. Stucky, *Nature* **1998**, *396*, 152.
[30] X. H. Wang, J. G. Li, H. Kamiyama, M. Katada, N. Ohashi, Y. Moriyoshi, T. Ishigaki, *J. Am. Chem. Soc.* **2005**, *127*, 10982.
[31] J. Lee, M. C. Orilall, S. C. Warren, M. Kamperman, F. J. Disalvo, U. Wiesner, *Nat. Mater.* **2008**, *7*, 222.
[32] A. Testino, I. R. Bellobono, V. Buscaglia, C. Canevali, M. D'Arienzo, S. Polizzi, R. Scotti, F. Morazzoni, *J. Am. Chem. Soc.* **2007**, *129*, 3564.
[33] D. Matthey, J. G. Wang, S. Wendt, J. Matthiesen, R. Schaub, E. Laegsgaard, B. Hammer, F. Besenbacher, *Science* **2007**, *315*, 1692.
[34] M. Zukalova, A. Zukal, L. Kavan, M. K. Nazeeruddin, P. Liska, M. Grätzel, *Nano Lett.* **2005**, *5*, 1789.
[35] O. K. Varghese, M. Paulose, C. A. Grimes, *Nat. Nanotechnol.* **2009**, *4*, 592.
[36] X. G. Han, Q. Kuang, M. S. Jin, Z. X. Xie, L. S. Zheng, *J. Am. Chem. Soc.* **2009**, *131*, 3152.
[37] H. G. Yang, C. H. Sun, S. Z. Qiao, J. Zou, G. Liu, S. C. Smith, H. M. Cheng, G. Q. Lu, *Nature* **2008**, *453*, 638.
[38] F. Sauvage, D. H. Chen, P. Comte, F. Z. Huang, L. P. Heiniger, Y. B. Cheng, R. A. Caruso, M. Grätzel, *ACS Nano* **2010**, *4*, 4420.
[39] D. H. Chen, F. Z. Huang, Y. B. Cheng, R. A. Caruso, *Adv. Mater.* **2009**, *21*, 2206.
[40] D. H. Chen, L. Cao, F. Z. Huang, P. Imperia, Y. B. Cheng, R. A. Caruso, *J. Am. Chem. Soc.* **2010**, *132*, 4438.
[41] D. H. Chen, F. Z. Huang, L. Cao, Y. B. Cheng, R. A. Caruso, *Chem. Eur. J.* **2012**, DOI: 10.1002/chem.201202539.
[42] F. Z. Huang, D. H. Chen, X. L. Zhang, R. A. Caruso, Y. B. Cheng, *Adv. Funct. Mater.* **2010**, *20*, 1301.
[43] F. Z. Huang, D. H. Chen, L. Cao, R. A. Caruso, Y. B. Cheng, *Energy Environ. Sci.* **2011**, *4*, 2803.
[44] F. Z. Huang, D. H. Chen, Q. Li, R. A. Caruso, Y. B. Cheng, *Appl. Phys. Lett.* **2012**, *100*, 123102.
[45] Y. Chen, F. Z. Huang, D. H. Chen, L. Cao, X. L. Zhang, R. A. Caruso, Y. B. Cheng, *ChemSusChem* **2011**, *4*, 1498.
[46] J. Y. Liao, B. X. Lei, D. B. Kuang, C. Y. Su, *Energy Environ. Sci.* **2011**, *4*, 4079.
[47] K. Yan, Y. Qiu, W. Chen, M. Zhang, S. Yang, *Energy Environ. Sci.* **2011**, *4*, 2168.
[48] J. Winkler, S. Marme, *J. Chromatogr., A* **2000**, *888*, 51.
[49] M. W. H. Pinkse, P. M. Uitto, M. J. Hilhorst, B. Ooms, A. J. R. Heck, *Anal. Chem.* **2004**, *76*, 3935.
[50] T. E. Thingholm, T. J. D. Jorgensen, O. N. Jensen, M. R. Larsen, *Nat. Protoc.* **2006**, *1*, 1929.
[51] J. Rappsilber, M. Mann, Y. Ishihama, *Nat. Protoc.* **2007**, *2*, 1896.
[52] Z. D. Lu, M. M. Ye, N. Li, W. W. Zhong, Y. D. Yin, *Angew. Chem. Int. Ed.* **2010**, *49*, 1862.
[53] Z. D. Lu, J. C. Duan, L. He, Y. X. Hu, Y. D. Yin, *Anal. Chem.* **2010**, *82*, 7249.
[54] H. Liu, Z. Bi, X.-G. Sun, R. R. Unocic, M. P. Paranthaman, S. Dai, G. M. Brown, *Adv. Mater.* **2011**, *23*, 3450.
[55] Y. G. Guo, Y. S. Hu, J. Maier, *Chem. Commun.* **2006**, 2783.
[56] Y. G. Guo, Y. S. Hu, W. Sigle, J. Maier, *Adv. Mater.* **2007**, *19*, 2087.
[57] J. S. Chen, Y. L. Tan, C. M. Li, Y. L. Cheah, D. Y. Luan, S. Madhavi, F. Y. C. Boey, L. A. Archer, X. W. Lou, *J. Am. Chem. Soc.* **2010**, *132*, 6124.
[58] J. Hu, M. Chen, X. S. Fang, L. W. Wu, *Chem. Soc. Rev.* **2011**, *40*, 5472.
[59] X. W. Lou, L. A. Archer, Z. C. Yang, *Adv. Mater.* **2008**, *20*, 3987.
[60] Q. Zhang, W. S. Wang, J. Goebl, Y. D. Yin, *Nano Today* **2009**, *4*, 494.

[61] F. Caruso, in *Topics in Current Chemistry*, Vol. *227* (Ed: M. Antonietti), Springer, Berlin **2003**, p. 145.
[62] U. Meyer, A. Larsson, H. P. Hentze, R. A. Caruso, *Adv. Mater.* **2002**, *14*, 1768.
[63] D. G. Shchukin, R. A. Caruso, *Chem. Mater.* **2004**, *16*, 2287.
[64] A. S. Deshpande, D. G. Shchukin, E. Ustinovich, M. Antonietti, R. A. Caruso, *Adv. Funct. Mater.* **2005**, *15*, 239.
[65] A. G. Dong, N. Ren, Y. Tang, Y. J. Wang, Y. H. Zhang, W. M. Hua, Z. Gao, *J. Am. Chem. Soc.* **2003**, *125*, 4976.
[66] K. F. Du, D. Yang, Y. Sun, *Ind. Eng. Chem. Res.* **2009**, *48*, 755.
[67] M. C. Kimling, R. A. Caruso, *J. Mater. Chem.* **2012**, *22*, 4073.
[68] N. Wu, H. H. Wei, L. Z. Zhang, *Environ. Sci. Technol.* **2012**, *46*, 419.
[69] M. Grun, C. Buchel, D. Kumar, K. Schumacher, B. Bidlingmaier, K. K. Unger, *Stud. Surf. Sci. Catal.* **2000**, *128*, 155.
[70] J. F. Chen, Z. J. Hua, Y. S. Yan, A. A. Zakhidov, R. H. Baughman, L. B. Xu, *Chem. Commun.* **2010**, *46*, 1872.
[71] F. Bai, D. S. Wang, Z. Y. Huo, W. Chen, L. P. Liu, X. Liang, C. Chen, X. Wang, Q. Peng, Y. D. Li, *Angew. Chem. Int. Ed.* **2007**, *46*, 6650.
[72] L. P. Liu, J. Hensel, R. C. Fitzmorris, Y. D. Li, J. Z. Zhang, *J. Phys. Chem. Lett.* **2010**, *1*, 155.
[73] Q. Zhang, J.-B. Joo, Z. Lu, M. Dahl, D. Oliveira, M. Ye, Y. Yin, *Nano Res.* **2011**, *4*, 103.
[74] S. H. Kim, Y. S. Cho, S. J. Jeon, T. H. Eun, G. R. Yi, S. M. Yang, *Adv. Mater.* **2008**, *20*, 3268.
[75] P. Tartaj, *Chem. Commun.* **2011**, *47*, 256.
[76] R. Rossmanith, C. K. Weiss, J. Geserick, N. Husing, U. Hormann, U. Kaiser, K. Landfester, *Chem. Mater.* **2008**, *20*, 5768.
[77] C. J. Brinker, Y. F. Lu, A. Sellinger, H. Y. Fan, *Adv. Mater.* **1999**, *11*, 579.
[78] C. J. Brinker, *MRS Bull.* **2004**, *29*, 631.
[79] C. Boissiere, D. Grosso, A. Chaumonnot, L. Nicole, C. Sanchez, *Adv. Mater.* **2011**, *23*, 599.
[80] Y. F. Lu, H. Y. Fan, A. Stump, T. L. Ward, T. Rieker, C. J. Brinker, *Nature* **1999**, *398*, 223.
[81] C.-K. Tsung, J. Fan, N. Zheng, Q. Shi, A. J. Forman, J. Wang, G. D. Stucky, *Angew. Chem. Int. Ed.* **2008**, *47*, 8682.
[82] L. Li, C. K. Tsung, Z. Yang, G. D. Stucky, L. D. Sun, J. F. Wang, C. H. Yan, *Adv. Mater.* **2008**, *20*, 903.
[83] Z. Jin, M. Xiao, Z. Bao, P. Wang, J. Wang, *Angew. Chem. Int. Ed.* **2012**, *51*, 6406.
[84] D. Grosso, G. Illia, E. L. Crepaldi, B. Charleux, C. Sanchez, *Adv. Funct. Mater.* **2003**, *13*, 37.
[85] H. Oveisi, N. Suzuki, A. Beitollahi, Y. Yamauchi, *J. Sol-Gel Sci. Technol.* **2010**, *56*, 212.
[86] P. Z. Araujo, V. Luca, P. B. Bozzano, H. L. Bianchi, G. Soler-Illia, M. A. Blesa, *ACS Appl. Mater. Interfaces* **2010**, *2*, 1663.
[87] Z. W. Wu, Y. F. Lu, *J. Sol-Gel Sci. Technol.* **2010**, *53*, 287.
[88] Y. Zhang, Y. Shi, Y.-H. Liou, A. M. Sawvel, X. Sun, Y. Cai, P. A. Holden, G. D. Stucky, *J. Mater. Chem.* **2010**, *20*.
[89] D. Hwang, H. Lee, S.-Y. Jang, S. M. Jo, D. Kim, Y. Seo, D. Y. Kim, *ACS Appl. Mater. Interfaces* **2011**, *3*, 2719.
[90] M. Ishida, S. W. Park, D. Hwang, Y. B. Koo, J. L. Sessler, D. Y. Kim, D. Kim, *J. Phys. Chem. C* **2011**, *115*, 19343.
[91] J. Xi, Q. Zhang, K. Park, Y. Sun, G. Cao, *Electrochim. Acta* **2011**, *56*, 1960.
[92] J. T. Xi, Q. F. Zhang, S. H. Xie, S. Yodyingyong, K. Park, Y. M. Sun, J. Y. Li, G. Z. Cao, *Nanosci. Nanotechnol. Lett.* **2011**, *3*, 690.
[93] B. Liu, K. Nakata, M. Sakai, H. Saito, T. Ochiai, T. Murakami, K. Takagi, A. Fujishima, *Langmuir* **2011**, *27*, 8500.
[94] S. Liu, G. Han, M. Shu, L. Han, S. Che, *J. Mater. Chem.* **2010**, *20*, 10001.
[95] T. Sugimoto, T. Kojima, *J. Phys. Chem. C* **2008**, *112*, 18760.
[96] T. Sugimoto, T. Kojima, *J. Phys. Chem. C* **2008**, *112*, 18437.
[97] T. Kojima, T. Sugimoto, *J. Phys. Chem. C* **2008**, *112*, 18445.
[98] S. Tanaka, D. Nogami, N. Tsuda, Y. Miyake, *J. Colloid Interface Sci.* **2009**, *334*, 188.
[99] N. Lakshminarasimhan, E. Bae, W. Choi, *J. Phys. Chem. C* **2007**, *111*, 15244.
[100] H. K. Yu, G.-R. Yi, J.-H. Kang, Y.-S. Cho, V. N. Manoharan, D. J. Pine, S.-M. Yang, *Chem. Mater.* **2008**, *20*, 2704.
[101] S. Y. Ryu, D. S. Kim, J. D. Jeon, S. Y. Kwak, *J. Phys. Chem. C* **2010**, *114*, 17440.
[102] X. C. Jiang, T. Herricks, Y. N. Xia, *Adv. Mater.* **2003**, *15*, 1205.
[103] J. B. Yin, L. Q. Xiang, X. P. Zhao, *Appl. Phys. Lett.* **2007**, *90*, 113112.
[104] S. Eiden-Assmann, J. Widoniak, G. Maret, *Chem. Mater.* **2004**, *16*, 6.
[105] A. F. Demirörs, A. Jannasch, P. D. J. van Oostrum, E. Schäffer, A. Imhof, A. van Blaaderen, *Langmuir* **2011**, *27*, 1626.
[106] K. Shiba, M. Ogawa, *Chem. Commun.* **2009**, 6851.
[107] K. Shiba, M. Ogawa, *J. Ceram. Soc. Jpn.* **2011**, *119*, 507.
[108] K. Shiba, K. Onaka, M. Ogawa, *RSC Adv.* **2012**, *2*, 1343.
[109] H. Zhang, Y. Han, X. Liu, P. Liu, H. Yu, S. Zhang, X. Yao, H. Zhao, *Chem. Commun.* **2010**, *46*, 8395.
[110] Z. Q. Sun, J. H. Kim, Y. Zhao, F. Bijarbooneh, V. Malgras, Y. Lee, Y. M. Kang, S. X. Dou, *J. Am. Chem. Soc.* **2011**, *133*, 19314.
[111] J. Q. Luo, L. Gao, *J. Alloys Compd.* **2009**, *487*, 763.
[112] H. M. Li, Y. S. Zeng, T. C. Huang, L. Y. Piao, Z. J. Yan, M. Liu, *Chem. Eur. J.* **2012**, *18*, 7525.
[113] H. M. Zhang, P. R. Liu, F. Li, H. W. Liu, Y. Wang, S. Q. Zhang, M. X. Guo, H. M. Cheng, H. J. Zhao, *Chem. Eur. J.* **2011**, *17*, 5949.
[114] M. M. Ye, Y. L. Yang, T. Q. Zhang, Y. Shao, C. Li, *Mater. Lett.* **2011**, *65*, 2384.
[115] C. X. Wang, L. W. Yin, L. Y. Zhang, Y. X. Qi, N. Lun, N. N. Liu, *Langmuir* **2010**, *26*, 12841.
[116] J. Zhou, G. L. Zhao, B. Song, G. R. Han, *CrystEngComm* **2011**, *13*, 2294.
[117] Z. K. Zheng, B. B. Huang, X. Y. Qin, X. Y. Zhang, Y. Dai, M. H. Whangbo, *J. Mater. Chem.* **2011**, *21*, 9079.
[118] H. X. Li, Z. F. Bian, J. Zhu, D. Q. Zhang, G. S. Li, Y. N. Huo, H. Li, Y. F. Lu, *J. Am. Chem. Soc.* **2007**, *129*, 8406.
[119] B. Chi, L. Zhao, T. Jin, *J. Phys. Chem. C* **2007**, *111*, 6189.
[120] S. K. Das, S. Darmakolla, A. J. Bhattacharyya, *J. Mater. Chem.* **2010**, *20*, 1600.
[121] W. Yang, J. Li, Y. Wang, F. Zhu, W. Shi, F. Wan, D. Xu, *Chem. Commun.* **2011**, *47*, 1809.
[122] S. W. Liu, J. G. Yu, M. Jaroniec, *J. Am. Chem. Soc.* **2010**, *132*, 11914.
[123] Z. Zheng, B. Huang, X. Qin, X. Zhang, Y. Dai, M. Jiang, P. Wang, M.-H. Whangbo, *Chem. Eur. J.* **2009**, *15*, 12576.
[124] J. Du, J. Zhang, D. J. Kang, *CrystEngComm* **2011**, *13*, 4270.
[125] Z. Sun, Z. Zhao, H. Zhao, M. Zheng, P. Du, J. Zhao, H. Fan, *J. Mater. Chem.* **2012**, *22*, 21965.
[126] Z. F. Bian, J. A. Zhu, J. Wen, F. L. Cao, Y. N. Huo, X. F. Qian, Y. Cao, M. Q. Shen, H. X. Li, Y. F. Lu, *Angew. Chem. Int. Ed.* **2011**, *50*, 1105.
[127] M. P. Hong, J. Y. Kim, K. Vemula, H. S. Kim, K. B. Yoon, *Chem. Commun.* **2012**, *48*, 4250.
[128] W. Q. Luo, R. F. Li, Y. S. Liu, X. Y. Chen, *J. Nanosci. Nanotechnol.* **2010**, *10*, 1693.
[129] I. G. Yu, Y. J. Kim, H. J. Kim, C. Lee, W. I. Lee, *J. Mater. Chem.* **2011**, *21*, 532.
[130] J. H. Pan, Z. Cai, Y. Yu, X. S. Zhao, *J. Mater. Chem.* **2011**, *21*, 11430.
[131] Y. J. Kim, M. H. Lee, H. J. Kim, G. Lim, Y. S. Choi, N.-G. Park, K. Kim, W. I. Lee, *Adv. Mater.* **2009**, *21*, 3668.
[132] Y.-C. Park, Y.-J. Chang, B.-G. Kum, E.-H. Kong, J. Y. Son, Y. S. Kwon, T. Park, H. M. Jang, *J. Mater. Chem.* **2011**, *21*, 9582.

[133] J. S. Lee, K. H. You, C. B. Park, *Adv. Mater.* **2012**, *24*, 1084.
[134] W. Q. Luo, R. F. Li, X. Y. Chen, *J. Phys. Chem. C* **2009**, *113*, 8772.
[135] P. Xiang, X. Li, H. Wang, G. Liu, T. Shu, Z. Zhou, Z. Ku, Y. Rong, M. Xu, L. Liu, M. Hu, Y. Yang, W. Chen, T. Liu, M. Zhang, H. Han, *Nanoscale Res. Lett.* **2011**, *6*, 606.
[136] Z. L. He, Z. F. Zhu, J. Q. Li, J. Q. Zhou, N. Wei, *J. Hazard. Mater.* **2011**, *190*, 133.
[137] W. Q. Luo, C. Y. Fu, R. F. Li, Y. S. Liu, H. M. Zhu, X. Y. Chen, *Small* **2011**, *7*, 3046.
[138] D. H. Chen, L. Cao, T. L. Hanley, R. A. Caruso, *Adv. Funct. Mater.* **2012**, *22*, 1966.
[139] W. Q. Luo, R. F. Li, G. K. Liu, M. R. Antonio, X. Y. Chen, *J. Phys. Chem. C* **2008**, *112*, 10370.
[140] X. Sun, Y. Liu, Q. Tai, B. Chen, T. Peng, N. Huang, S. Xu, T. Peng, X.-Z. Zhao, *J. Phys. Chem. C* **2012**, *116*, 11859.
[141] D. K. Roh, J. A. Seo, W. S. Chi, J. K. Koh, J. H. Kim, *J. Mater. Chem.* **2012**, *22*, 11079.
[142] J. Zhang, X. H. Liu, S. R. Wang, S. H. Wu, B. Q. Cao, S. H. Zheng, *Powder Technol.* **2012**, *217*, 585.
[143] Z. Ali, S. N. Cha, J. I. Sohn, I. Shakir, C. Yan, J. M. Kim, D. J. Kang, *J. Mater. Chem.* **2012**, *22*, 17625.
[144] H. D. Kurland, C. Stotzel, J. Grabow, I. Zink, E. Muller, G. Staupendahl, F. A. Muller, *J. Am. Ceram. Soc.* **2010**, *93*, 1282.
[145] H. Chang, S. J. Kim, H. D. Jang, J. W. Choi, *Colloids Surf., A* **2008**, *313-314*, 282.
[146] H. K. Park, D. K. Kim, C. H. Kim, *J. Am. Ceram. Soc.* **1997**, *80*, 743.
[147] C. H. Cho, D. K. Kim, D. H. Kim, *J. Am. Ceram. Soc.* **2003**, *86*, 1138.
[148] J. G. Li, C. C. Tang, D. Li, H. Haneda, T. Ishigaki, *J. Am. Ceram. Soc.* **2004**, *87*, 1358.
[149] H.-E. Wang, L.-X. Zheng, C.-P. Liu, Y.-K. Liu, C.-Y. Luan, H. Cheng, Y. Y. Li, L. Martinu, J. A. Zapien, I. Bello, *J. Phys. Chem. C* **2011**, *115*, 10419.
[150] A. Pringuet, C. Pagnoux, A. Videcoq, J. F. Baumard, *Langmuir* **2008**, *24*, 10702.
[151] A. Pringuet, F. Belounis, C. Pagnoux, *J. Am. Ceram. Soc.* **2011**, *94*, 729.
[152] A. Pringuet, C. Pagnoux, A. Videcoq, J. F. Baumard, *Microporous Mesoporous Mater.* **2011**, *140*, 17.
[153] Z. T. Jiang, Y. M. Zuo, *Anal. Chem.* **2001**, *73*, 686.
[154] A. Leitner, *TrAC, Trends Anal. Chem.* **2010**, *29*, 177.
[155] J. Tang, P. Yin, X. H. Lu, D. W. Qi, Y. Mao, C. H. Deng, P. Y. Yang, X. M. Zhang, *J. Chromatogr., A* **2010**, *1217*, 2197.
[156] M. R. Larsen, T. E. Thingholm, O. N. Jensen, P. Roepstorff, T. J. D. Jorgensen, *Mol. Cell. Proteomics* **2005**, *4*, 873.
[157] J. Wu, Q. Shakey, W. Liu, A. Schuller, M. T. Follettie, *J. Proteome Res.* **2007**, *6*, 4684.
[158] Q. R. Li, Z. B. Ning, J. S. Tang, S. Nie, R. Zeng, *J. Proteome Res.* **2009**, *8*, 5375.
[159] G. N. Zhu, Y. G. Wang, Y. Y. Xia, *Energy Environ. Sci.* **2012**, *5*, 6652.
[160] D. Deng, M. G. Kim, J. Y. Lee, J. Cho, *Energy Environ. Sci.* **2009**, *2*, 818.
[161] K. Saravanan, K. Ananthanarayanan, P. Balaya, *Energy Environ. Sci.* **2010**, *3*, 939.
[162] J. F. Ye, W. Liu, J. G. Cai, S. A. Chen, X. W. Zhao, H. H. Zhou, L. M. Qi, *J. Am. Chem. Soc.* **2011**, *133*, 933.
[163] Q. F. Zhang, T. R. Chou, B. Russo, S. A. Jenekhe, G. Z. Cao, *Angew. Chem. Int. Ed.* **2008**, *47*, 2402.
[164] Q. F. Zhang, T. R. Chou, B. Russo, S. A. Jenekhe, G. Z. Cao, *Adv. Funct. Mater.* **2008**, *18*, 1654.
[165] C. R. Ke, J. M. Ting, *J. Power Sources* **2012**, *208*, 316.
[166] C.-R. Ke, L.-C. Chen, J.-M. Ting, *J. Phys. Chem. C* **2012**, *116*, 2600.
[167] L. Sun, Y. Qin, Q. Q. Cao, B. Q. Hu, Z. W. Huang, L. Ye, X. F. Tang, *Chem. Commun.* **2011**, *47*, 12628.
[168] K. L. Frindell, M. H. Bartl, A. Popitsch, G. D. Stucky, *Angew. Chem. Int. Ed.* **2002**, *41*, 959.
[169] Y. C. Cheng, J. J. Guo, X. H. Liu, A. H. Sun, G. J. Xu, P. Cui, *J. Mater. Chem.* **2011**, *21*, 5051.
[170] J. B. Yin, X. P. Zhao, L. Q. Xiang, X. Xia, Z. S. Zhang, *Soft Matter* **2009**, *5*, 4687.
[171] R. Shen, X. Z. Wang, Y. Lu, D. Wang, G. Sun, Z. X. Cao, K. Q. Lu, *Adv. Mater.* **2009**, *21*, 4631.
[172] X. X. Zou, G. D. Li, Y. N. Wang, J. Zhao, C. Yan, M. Y. Guo, L. Li, J. S. Chen, *Chem. Commun.* **2011**, *47*, 1066.
[173] L. S. Zhong, J. S. Hu, Z. M. Cui, L. J. Wan, W. G. Song, *Chem. Mater.* **2007**, *19*, 4557.
[174] F. Niu, Y. Jiang, W. G. Song, *Nano Res.* **2010**, *3*, 757.
[175] D. Wen, S. J. Guo, J. F. Zhai, L. Deng, W. Ren, S. J. Dong, *J. Phys. Chem. C* **2009**, *113*, 13023.
[176] E. Mine, M. Hirose, D. Nagao, Y. Kobayashi, M. Konno, *J. Colloid Interface Sci.* **2005**, *291*, 162.
[177] L. S. Zhong, J. S. Hu, L. J. Wan, W. G. Song, *Chem. Commun.* **2008**, 1184.
[178] K. C. W. Wu, Y. Yamauchi, C. Y. Hong, Y. H. Yang, Y. H. Liang, T. Funatsu, M. Tsunoda, *Chem. Commun.* **2011**, *47*, 5232.